 CMC, vol.44, no.3, pp.167-204, 2014

Bending, Free Vibration and Buckling Analysis of Functionally Graded Plates via Wavelet Finite Element Method

Hao Zuo[1,2], **Zhibo Yang**[1,2,3], **Xuefeng Chen**[1,2], **Yong Xie**[4] **and Xingwu Zhang**[1,2]

Abstract: Following previous work, a wavelet finite element method is developed for bending, free vibration and buckling analysis of functionally graded (FG) plates based on Mindlin plate theory. The functionally graded material (FGM) properties are assumed to vary smoothly and continuously throughout the thickness of plate according to power law distribution of volume fraction of constituents. This article adopts scaling functions of two-dimensional tensor product BSWI to form shape functions. Then two-dimensional FGM BSWI element is constructed based on Mindlin plate theory by means of two-dimensional tensor product BSWI. The proposed two-dimensional FGM BSWI element possesses the advantages of high convergence, high accuracy and reliability with fewer degrees of freedoms on account of the excellent approximation property of BSWI. Numerical examples concerning various length-to-thickness ratios, volume fraction indexes, aspect ratios and boundary conditions are carried out for bending, free vibration and buckling problems of FG plates. These comparison examples demonstrate the accuracy and reliability of the proposed WFEM method comparing with the exact and referential solutions available in literatures.

Keywords: Functionally graded plates, Wavelet finite element method, Mindlin plate theory, Bending, free vibration and buckling analysis.

1 Introduction

Over the past few decades, the science and technology mainly focus on homogeneous materials such as metal, alloy, ceramic and polymer, etc. However, the tradi-

[1] The State Key Laboratory for Manufacturing Systems Engineering, Xi'an, P.R. China.
[2] School of Mechanical Engineering, Xi'an Jiaotong University, Xi'an, P.R. China.
[3] Corresponding author. Tel: +86 29 82667963; Fax: +86 29 82663689.
E-mail: yangbo-5-7@163.com
[4] State Key Laboratory of Strength and Vibration for Mechanical Struictures, School of Aerospace.

tional homogeneous materials are face with the challenge of ultrahigh temperature resistance with the rapid development of aerospace industry. Functionally graded materials (FGM) are new advanced composites firstly proposed as heat-shielding structural materials in space applications by Japanese material scientists in 1984 [Koizumi (1997)]. Generally, FGM are comprised of ceramic and metal with material properties varying smoothly and continuously throughout one surface to another. The smooth and continuity of FGM properties are able to effectively reduce the influence of interface and eliminate high interfacial stress. These excellent characteristics make FGM be widely used in the areas of aircraft, space vehicle, nuclear, mechanical, optical, chemical and biomechanical and other engineering structures. Due to the increasing applications of FGM in engineering structures, the theoretical research of FGM structures has attracted considerable researchers' attention.

Functionally graded (FG) plate structures, as one of basic structures in engineering areas, play a very important role in engineering practical and theoretical analysis [Akgoz and Civalek (2013a)]. Hence, various plate theories are proposed for problems of FG plates. The classical plate theory (CPT), also named Kirchhoff plate theory, neglects the transverse shear deformation and rotary inertia terms. Shen [Yang and Shen (2001)] dealt with the dynamic response of initially stressed thin FG plates subjected to impulsive lateral loads based on CPT. The elastic foundation was considered in their research. Abrate [Abrate (2008)] adopted CPT to investigate free vibration of FG plates with simply supported and clamped boundary conditions. Eslami [Shariat et al. (2005)] investigated the buckling analysis of FG plates based on CPT. Saidi [Mohammadi et al. (2010); Baferani et al. (2011)] presented an analytical method for free vibration and buckling analysis of thin FG plates based on CPT. It is observed that the CPT gives satisfactory solutions for thin plates.

However, the effect of transverse shear deformation becomes remarkable with the increasing thickness of plates. For this reason, the first order shear deformation plate theory (FSDT) also named Mindlin plate theory was proposed for moderately thick plates by Mindlin [Mindlin (1951); Mindlin et al. (1955); Civalek and Acar (2007)]. The FSDT can be considered as an extension of the Timoshenko theory to beam. Unlike Kirchhoff plate theory, this plate theory takes the effect of transverse shear deformations and rotational inertia into account which greatly improves the calculation accuracy of moderately thick plate (length/thickness $<$ 10 or 20). Although high efficiency and simplicity of FSDT, shear correction factors are required to correct variation of transverse shear stress and shear strain through the thickness [Akgoz and Civalek (2013b)]. Then various higher order shear deformation plate theories (HSDTs) are proposed for the problems of thick FG plates. These HSDTs also give satisfactory solutions for thick plates without requiring shear correction

factors.

Kitipornchai [Yang et al. (2005)] studied the buckling analysis of FG plates resting on elastic foundations based on FSDT. Liew [Zhao et al. (2009b); Zhao et al. (2009a)] employed FSDT to investigate the free vibration, mechanical and thermal buckling analysis of FG plates using element-free *kp*-Ritz method. Then a local Kriging meshless method was proposed for free vibration of FG plates based on FSDT by Liew [Zhu and Liew (2011)]. A group of satisfactory solutions for square, skew, quadrilateral plates and plates with holes are given in their literatures. An analytical solution based on FSDT was proposed for free vibration of moderately thick FG plates without or resting elastic foundations by Hashemi [Hosseini-Hashemi et al. (2010); Hosseini-Hashemi et al. (2011a)]. The benchmark solutions of FG plates with SSSS, SSSC, SCSC, SCSF, SSSF, SFSF are reported in their literatures. Singha [Singha et al. (2011)] formulated a four-node high precision plate bending element to analyze the deflections and stresses of FG plates subjected to a sinusoidal or uniformly distributed loads. Choi [Thai and Choi (2013)] developed a simple FSDT for the bending and free vibration analysis of FG plates. Zenkour [Zenkour (2005b); Zenkour (2005a)] proposed sinusoidal shear deformation plate theory (SSDT) for bending, buckling and free vibration analysis of FG plates. After then Tounsi [Ameur et al. (2011); Merdaci et al. (2011); Tounsi et al. (2013)] and Thai [Thai and Vo (2013)] developed SSDT for similar problems of FG plates. Wu [Wu and Li (2010)] employed third order shear deformation theory (TSDT) to investigate the static behaviors of FG plates. A new exact closed-form procedure based on Reddy's TSDT was proposed for free vibration of FG plates by Hashemi [Hosseini-Hashemi et al. (2011b)]. The buckling analysis of FG plates are studied by Eslami [Shariat and Eslami (2007)] and Cheng [Cheng and Batra (2000)] based on TSDT. Liew [Liew et al. (2003)] employed Reddy's high order shear deformation plate theory (HSDT) to study the postbuckling response of piezoelectric FG plates. The thermal, mechanical and electrical buckling are considered in their study. An analytical solution based on HSDT was proposed for nonlinear vibration and dynamic response of FG plates in thermal environments by Shen [Huang and Shen (2004)]. Ferreira and his co-workers employed SSDT [Neves et al. (2012)], TSDT [Ferreira et al. (2007); Ferreira et al. (2005)] and HSDT [Neves et al. (2013)] for static, free vibrations and buckling analysis of isotropic and sandwich FG plates. These literatures pointed that the effect of thickness stretching showed significance in thicker plates. Natural frequencies and buckling loads of FG plates were obtained by Matsunaga [Matsunaga (2008)] and Tzou [Chen et al. (2009)] using 2D HSDT and HSDT, respectively. Saidi [Bodaghi and Saidi (2010)] just considered the buckling problems of FG plates in the framework of HSDT. However, it is the first time to consider the buckling analysis of FG plates with various bound-

ary conditions. The FG plates resting on a Winkler-Pasternak elastic foundation were considered by Tounsi [Benyoucef et al. (2010)] and Atmane [Atmane et al. (2010)]. They employed HSDT for static response and free vibration of FG plates, respectively. Singh [Talha and Singh (2010)] employed HSDT for static response and free vibration of FG plate. The same work has also been done by Natarajan [Natarajan and Manickam (2012)]. They constructed a C^0 8-noded quadrilateral plates element with 13 degrees of freedom per node for the problems of FG plates. A higher order shear and normal deformable plates theory (HOSNDPT) has been proposed for static analysis of FG plates by Xiao [Gilhooley et al. (2007)] and Batra [Qian et al. (2004)]. Recently, Dong [Dong et al. (2014a)] developed a simple locking-alleviated 3D 8-node mixed-collocation C^0 finite element for FG plates and shells based on [Dong et al. (2014b)]. The widely-available theories of elasticity were employed for modeling FG structures without using HSDT in their works which solved the over-integration problem for FGM structures.

Although various numerical methods have already been proposed for bending, free vibration and buckling analysis of FG plates, the analytical solutions for problems of FG plates are rarely reported. In addition, traditional numerical methods, such as finite element method, often require more computing grids due to the continuous variation of material properties in FGM. According to the literatures mentioned before, literatures concerning bending problems, free vibration problems and buckling problems of FG plates at the same time are very few. Their attentions mainly focus on one or two of these problems. Hence, it is very meaningful and useful to propose an accurate and effective numerical method for deriving exact and comprehensive closed form solutions of FG plates.

Nowadays, High performance numerical computer methods, such as boundary element method (BEM) [Hall (1994)], meshless local Petrov-Galerkin (MLPG) method [Atluri and Zhu (1998)], local boundary integral equation (LBIE) method [Atluri et al. (2000)], the discontinuous Galerkin method [Hartmann and Houston (2002)] and hybrid/mixed finite element method [Dong and Atluri (2011)], play a crucial role for numerical simulation problems. The wavelet finite element method (WFEM) is another powerful analysis tool developed in recently [Chen and Wu (1995); Chen and Wu (1996); Zhong and Xiang (2011)]. The WFEM employs a series of scaling functions as approximating functions. Compared with other wavelets, B-spline wavelet on the interval (BSWI) basis has the excellent characteristics of compact support, smoothness and symmetry in addition to the multiresolution analysis. Moreover, BSWI element, as a type of generalized spline finite element method, inherits the superiority of spline for structural analysis. Above all, it has explicit expressions so the coefficient integration and differentiation can be calculated conveniently. Hence, the WFEM employing BSWI as approximat-

ing functions is the best choice for solving bending, free vibration and buckling problems of FG plates. In previous studies about BSWI elements, the main investigations are focused on the elements with uniform density and Young's modulus on the out of plane direction, which induces the decoupling of the displacements between in plane and out of plane [Xiang et al. (2006); Jiawei et al. (2008); Yang et al. (2013)]. Following previous work [Zuo et al. (in press)], the WFEM is extended to solve the FG plate problems in this paper.

Due to the excellent characteristics of BSWI, this paper adopts BSWI to investigate the bending, free vibration and buckling analysis of FG plates. The outline of this paper is organized as follows. The introduction of FGM is briefly presented in section 2. The formulation of FGM BSWI plate element and the equations of bending, free vibration and buckling of FG plate are derived in section 3. Various numerical examples and comparisons are provided to demonstrate the accuracy and efficiency of the constructed FGM BSWI element for FG plates in section 4.

2 Functionally graded material

A flat and moderately thick rectangular FG plate of length a, width b and thickness h is considered and depicted in Fig.1. The Cartesian coordinate system is defined on the neutral surface of plate where x-axis is taken along the length direction, y-axis in the width direction and z-axis in the thickness direction.

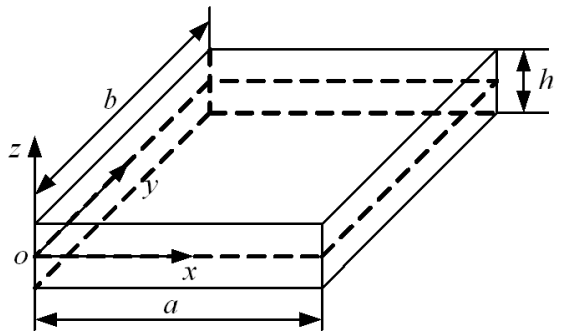

Figure 1: Geometry and coordinates of rectangular FG plate.

Generally, the FG plate is always made of ceramic and metal and the material properties of FG plate, such as Young's modulus E, mass density ρ and Poisson's ratio μ, are assumed to vary continuously throughout the thickness of plate according to the power law distribution of volume fraction of constituents. According to the rule

of mixture, the effective material properties P can be expressed as

$$P = P_m V_m + P_c V_c \tag{1}$$

where P_m, P_c, V_m and V_c are defined as the material properties and volume fractions of metal and ceramic, respectively. The volume fractions of two constituent materials are assumed as

$$V_m + V_c = 1 \tag{2}$$

In this paper, the volume fraction for a plate with referential surface at its neutral surface can be written as

$$V_c = \left(\frac{z}{h} + \frac{1}{2}\right)^n \tag{3}$$

where n is a non-negative exponent named volume fraction index. The volume fraction index n dictates the material variation profile thickness of FG plate. Then the effective material properties of FG plate which consists of two constituent materials can be expressed as

$$\begin{cases} E(z) = (E_c - E_m)\left(\dfrac{z}{h} + \dfrac{1}{2}\right)^n + E_m \\ \rho(z) = (\rho_c - \rho_m)\left(\dfrac{z}{h} + \dfrac{1}{2}\right)^n + \rho_m \\ \mu(z) = (\mu_c - \mu_m)\left(\dfrac{z}{h} + \dfrac{1}{2}\right)^n + \mu_m \end{cases} \tag{4}$$

where the subscripts c and m represent ceramic and metal, respectively. The material properties of metal and ceramic used in FG plates are listed in Table 1.

The effective Young's modulus through the thickness of Al/Al_2O_3 plate with various volume fraction indexes is shown in Fig. 2. to clarify the behavior of FG plate. It is clearly that the bottom surface (z = -h/2) of FG plate is metal rich while the top surface ($z = h/2$) material of FG plate is ceramic rich. And the material properties vary continuously and smoothly from metal rich to ceramic rich with different volume fraction indexes. Moreover, the FG plate is fully ceramic (Al_2O_3) and metal (Al) for n = 0 and $n = \infty$, respectively.

3 Formulation of B-spline wavelet on the interval Mindlin plate element

3.1 Two-dimensional tensor product BSWI on the interval [0, 1]

The mth order B-spline functions need to be construed on the interval [0, 1] due to any one-dimensional function $f(x)$ on the interval [a, b] can be transformed to

Table 1: Material properties of metal and ceramic used in FG plates.

Material	Properties		
	E(Pa)	μ	ρ (kg/m^3)
Aluminum (Al)	70×10^9	0.30	2707
Stainless Steel(SUS304)	207.78×10^9	0.3177	8166
Alumina (Al_2O_3)	380×10^9	0.30	3800
Zirconia (ZrO_2)	151×10^9	0.30	3000
Silicon Nitride (Si_3N_4)	322.21×10^9	0.24	2370
Silicon Carbide (SiC)	420×10^9	0.17	3210

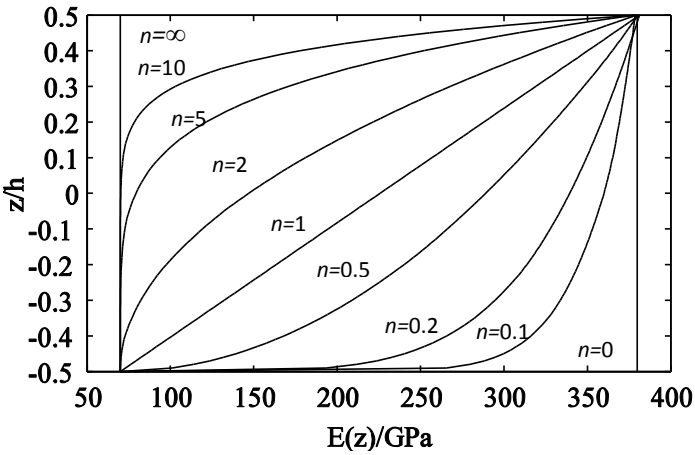

Figure 2: The effective Young' modulus through the thickness of Al/Al_2O_3 plate with various volume fraction indexes.

the standard interval [0, 1] by means of a linear mapping $\xi = (x-a)/(b-a)$. In order to meet at least one inner wavelet on the interval [0, 1], the condition should be satisfied as

$$2^j \geq 2m-1 \tag{5}$$

where j is the scale number of BSWI.

For any j scale mth order BSWI, which can be written as BSWI m_j, the scaling

functions $\phi^j_{m,k}(\xi)$ can be calculated by the following formula [Xiang et al. (2007)]

$$\phi^j_{m,k}(\xi)=\begin{cases}\phi^l_{m,k}(2^{j-l}\xi),\ k=-m+1,\cdots,-1 & \text{(0 boundary scaling functions)}\\ \phi^l_{m,2^j-m-k}(1-2^{j-l}\xi),\ k=2^j-m+1,\cdots,2^j-1 & \text{(1 boundary scaling functions)}\\ \phi^l_{m,0}(2^{j-l}\xi-2^{-l}k),\ k=0,\cdots,2^j-m & \text{(inner scaling functions)}\end{cases} \tag{6}$$

Let j_0 be the scale as the condition Eq. (5) is satisfied. Then for each $j > j_0$, let l = 0, the scaling functions can be obtacined through Eq. (6). Therefore, the scaling functions on the interval [0, 1] can be written in vector form as

$$\begin{aligned}\boldsymbol{\Phi}_1 &= [\phi^j_{m,-m+1}(\xi),\phi^j_{m,-m+2}(\xi),\cdots,\phi^j_{m,2^j-1}(\xi)]\\ \boldsymbol{\Phi}_2 &= [\phi^j_{m,-m+1}(\eta),\phi^j_{m,-m+2}(\eta),\cdots,\phi^j_{m,2^j-1}(\eta)]\end{aligned} \tag{7}$$

where ξ and η depict the normalized x and y coordinates, respectively.

Tensor product is the best way to construct two-dimensional BSWI from one-dimensional BSWI. It is assumed that two-dimensional tensor product of BSWI at scale j of L_2 (R^2) can be constructed by multi-resolution approximation space $F_j = V^1_j \otimes V^2_j$ and the scaling functions of two-dimensional BSWI are

$$\boldsymbol{\Phi} = \boldsymbol{\Phi}_1 \otimes \boldsymbol{\Phi}_2 \tag{8}$$

where $\boldsymbol{\Phi}_1$ and $\boldsymbol{\Phi}_2$ are two different variations in scaling functions given by Eq. (7), the symbol $\otimes$ denotes the kronecker function. Some selected $BSWI4_3$ scaling functions are presented in Fig.3 to clarify the BSWI shape function.

3.2 The theory formulation of Mindlin plate

According to Mindlin plate theory, normal to the undeformed middle plane of the plate remains straight, but not normal to the deformed middle surface. In Cartesian coordinate system, the assumed displacement field is defined as follows

$$u(x,\mathrm{y},z,t) = u_0(x,y,t) - z\theta_x(x,y,t) \tag{9}$$

$$v(x,\mathrm{y},z,t) = v_0(x,y,t) - z\theta_y(x,y,t) \tag{10}$$

$$w(x,\mathrm{y},z,t) = w_0(x,y,t) \tag{11}$$

where u_0, v_0, w_0 are the x-direction, y-direction and z-direction displacements of the plate on the neutral plane, respectively, θ_x and θ_y are the rotations of a transverse normal about axis y and x, and t denotes time.

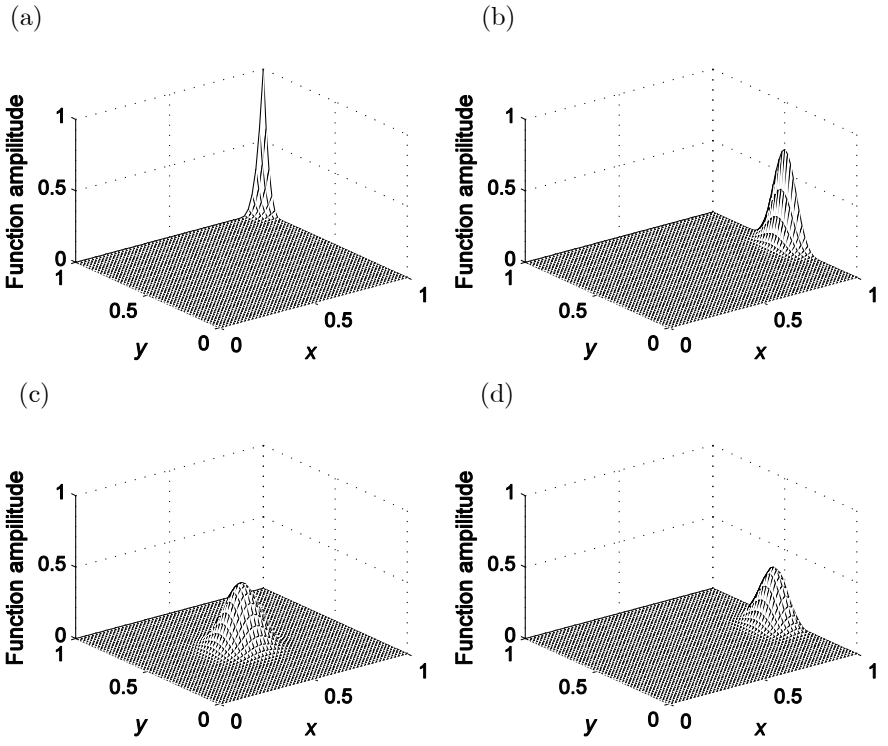

Figure 3: (a-d) some typical two-dimensional BSWI4$_3$ scaling functions.

Based on the small deformations assumption, the bending strains ε_{xx}, ε_{yy} and γ_{xy} can be written as

$$\varepsilon_{xx} = \frac{\partial u}{\partial x} = \frac{\partial u_0(x,y,t)}{\partial x} - z\frac{\partial \theta_x(x,y,t)}{\partial x} \tag{12}$$

$$\varepsilon_{yy} = \frac{\partial v}{\partial y} = \frac{\partial v_0(x,y,t)}{\partial y} - z\frac{\partial \theta_y(x,y,t)}{\partial y} \tag{13}$$

$$\gamma_{xy} = \frac{\partial u}{\partial y} + \frac{\partial v}{\partial x} = \frac{\partial u_0(x,y,t)}{\partial y} + \frac{\partial v_0(x,y,t)}{\partial x} - z\frac{\partial \theta_x(x,y,t)}{\partial y} - z\frac{\partial \theta_y(x,y,t)}{\partial x} \tag{14}$$

while the transverse shear strains γ_{xz} and γ_{yz} can be written as

$$\gamma_{xz} = \frac{\partial w}{\partial x} + \frac{\partial u}{\partial z} = \frac{\partial w_0(x,y,t)}{\partial x} - \theta_x(x,y,t) \tag{15}$$

$$\gamma_{yz} = \frac{\partial w}{\partial y} + \frac{\partial v}{\partial z} = \frac{\partial w_0(x,y,t)}{\partial y} - \theta_y(x,y,t) \tag{16}$$

According to the Mindlin plate theory, the total strain energy of Mindlin plate consists of two parts

$$U = U_\varepsilon + U_\gamma \tag{17}$$

where

$$U_\varepsilon = \frac{1}{2}\int_V \sigma\varepsilon \mathrm{d}V \tag{18}$$

$$U_\gamma = \frac{1}{2}\int_V \tau\gamma \mathrm{d}V \tag{19}$$

where ε represents the bending strain which can be written as $\varepsilon = [\varepsilon_{xx}, \varepsilon_{yy}, \gamma_{xy}]^T$ and γ represents the transverse shear strain which can be written as $\gamma = [\gamma_{xz}, \gamma_{yz}]^T$. According to the Hooke's law, the bending stress σ and transverse shear stress τ are obtained as

$$\sigma = D_b\varepsilon \tag{20}$$

$$\tau = D_s\gamma \tag{21}$$

where D_b and D_s are corresponding elasticity matrixes which can be defined as

$$D_b = \frac{E(z)}{1-\mu^2}\begin{bmatrix} 1 & \mu & 0 \\ \mu & 1 & 0 \\ 0 & 0 & \frac{1-\mu}{2} \end{bmatrix} \tag{22}$$

$$D_s = \frac{kE(z)}{2(1+\mu)}\begin{bmatrix} 1 & 0 \\ 0 & 1 \end{bmatrix} \tag{23}$$

where $E(z)$ is the Young's modulus varying continuously throughout the thickness direction, μ is the Poisson's ratio and the variable k is known as the shear correction factor.

The kinetic energy for Mindlin plate consists of two parts. One of them is related with translations and the other is related with rotations. Then the kinetic energy can be obtained as

$$T = \frac{1}{2}\int_V \rho(z)\left\{\left(\frac{\partial u}{\partial t}\right)^2 + \left(\frac{\partial v}{\partial t}\right)^2 + \left(\frac{\partial w}{\partial t}\right)^2\right\}\mathrm{d}V \tag{24}$$

in which $\rho(z)$ denotes the mass density varying continuously throughout the thickness direction. Then the variational energy function can be defined as the difference between the strain energy and the kinetic energy

$$\Pi = U - T \tag{25}$$

3.3 The formulation of FGM BSWI plate elements

In Mindlin plate element, the displacements and rotations can be interpolated by tensor product of BSWI scaling functions, respectively. The displacement fields can been derived as follow

$$u = \mathbf{\Phi T} \boldsymbol{u} \quad v = \mathbf{\Phi T} \boldsymbol{v} \quad w = \mathbf{\Phi T} \boldsymbol{w} \quad \theta_x = \mathbf{\Phi T} \boldsymbol{\theta}_x \quad \theta_y = \mathbf{\Phi T} \boldsymbol{\theta}_y \tag{26}$$

where $\mathbf{u}$, $\boldsymbol{v}$, $\mathbf{w}$, θ_x, θ_y are the displacement vectors in BSWI scaling space, respectively, and $\mathbf{T}$ is the BSWI element transform matrix. $\mathbf{T}$ is obtained by the tensor product as $\mathbf{T} = \mathbf{T}_1 \otimes \mathbf{T}_2$ which can be written as

$$\mathbf{T}_1 = [\mathbf{\Phi}^T(\xi_1)\ \mathbf{\Phi}^T(\xi_2) \cdots \mathbf{\Phi}^T(\xi_{n+1})]^{-\mathrm{T}} \tag{27}$$

$$\mathbf{T}_2 = [\mathbf{\Phi}^T(\eta_1)\ \mathbf{\Phi}^T(\eta_2) \cdots \mathbf{\Phi}^T(\eta_{n+1})]^{-\mathrm{T}} \tag{28}$$

Substitute the displacement field Eqs. (26) into Eqs. (12-16) and the results are

$$\boldsymbol{\varepsilon} = \mathbf{B}_b \boldsymbol{d} = \begin{bmatrix} \frac{\partial}{\partial x} & 0 & 0 & -z\frac{\partial}{\partial x} & 0 \\ 0 & \frac{\partial}{\partial y} & 0 & 0 & -z\frac{\partial}{\partial y} \\ \frac{\partial}{\partial y} & \frac{\partial}{\partial x} & 0 & -z\frac{\partial}{\partial y} & -z\frac{\partial}{\partial x} \end{bmatrix} \boldsymbol{d} \tag{29}$$

$$\boldsymbol{\gamma} = \mathbf{B}_s \boldsymbol{d} = \begin{bmatrix} 0 & 0 & \frac{\partial}{\partial x} & -1 & 0 \\ 0 & 0 & \frac{\partial}{\partial y} & 0 & -1 \end{bmatrix} \boldsymbol{d} \tag{30}$$

where $\boldsymbol{d}$ can be expressed as $\boldsymbol{d}$=$[u \quad v \quad w \quad \theta_x \quad \theta_y]^T$.

3.3.1 Bending analysis of BSWI Mindlin plate

In this section, the bending analysis of Mindlin plate is formulated and implemented. According to Hamilton's principle, the equation of motions for bending analysis of Mindlin plate can be expressed as

$$\delta\Pi = \int_{t_1}^{t_2} (\delta U - \delta W)\mathrm{d}t = 0 \tag{31}$$

Substituting Eqs. (29-30) into Eq. 31, the basic governing equation of bending problem is obtained as

$$\mathbf{K}\boldsymbol{d} = \boldsymbol{F} \tag{32}$$

where $\mathbf{K}$ is stiffness matrix, $\boldsymbol{F}$ is force vector.

The stiffness matrix $\mathbf{K}$ is defined by the summation of two parts

$$\mathbf{K} = \mathbf{K}_\varepsilon + \mathbf{K}_\gamma \tag{33}$$

$$\mathbf{K}_\varepsilon = \begin{bmatrix} \mathbf{K}_\varepsilon^{11} & \mathbf{K}_\varepsilon^{12} & 0 & \mathbf{K}_\varepsilon^{14} & \mathbf{K}_\varepsilon^{15} \\ \mathbf{K}_\varepsilon^{21} & \mathbf{K}_\varepsilon^{22} & 0 & \mathbf{K}_\varepsilon^{24} & \mathbf{K}_\varepsilon^{25} \\ 0 & 0 & 0 & 0 & 0 \\ \mathbf{K}_\varepsilon^{41} & \mathbf{K}_\varepsilon^{42} & 0 & \mathbf{K}_\varepsilon^{44} & \mathbf{K}_\varepsilon^{45} \\ \mathbf{K}_\varepsilon^{51} & \mathbf{K}_\varepsilon^{52} & 0 & \mathbf{K}_\varepsilon^{54} & \mathbf{K}_\varepsilon^{55} \end{bmatrix} \tag{34}$$

where

$$\mathbf{K}_\varepsilon^{11} = A_{11} \times (\mathbf{\Gamma}_x^{1,1} \otimes \mathbf{\Gamma}_y^{0,0}) + A_{33} \times (\mathbf{\Gamma}_x^{0,0} \otimes \mathbf{\Gamma}_y^{1,1});$$

$$\mathbf{K}_\varepsilon^{12} = A_{12} \times (\mathbf{\Gamma}_x^{1,0} \otimes \mathbf{\Gamma}_y^{0,1}) + A_{33} \times (\mathbf{\Gamma}_x^{0,1} \otimes \mathbf{\Gamma}_y^{1,0});$$

$$\mathbf{K}_\varepsilon^{14} = -B_{11} \times (\mathbf{\Gamma}_x^{1,1} \otimes \mathbf{\Gamma}_y^{0,0}) - B_{33} \times (\mathbf{\Gamma}_x^{0,0} \otimes \mathbf{\Gamma}_y^{1,1});$$

$$\mathbf{K}_\varepsilon^{15} = -B_{12} \times (\mathbf{\Gamma}_x^{1,0} \otimes \mathbf{\Gamma}_y^{0,1}) - B_{33} \times (\mathbf{\Gamma}_x^{0,1} \otimes \mathbf{\Gamma}_y^{1,0});$$

$$\mathbf{K}_\varepsilon^{21} = (\mathbf{K}_\varepsilon^{12})^T; \quad \mathbf{K}_\varepsilon^{22} = A_{11} \times (\mathbf{\Gamma}_x^{0,0} \otimes \mathbf{\Gamma}_y^{1,1}) + A_{33} \times (\mathbf{\Gamma}_x^{1,1} \otimes \mathbf{\Gamma}_y^{0,0});$$

$$\mathbf{K}_\varepsilon^{24} = (\mathbf{K}_\varepsilon^{15})^T; \quad \mathbf{K}_\varepsilon^{25} = -B_{11} \times (\mathbf{\Gamma}_x^{0,0} \otimes \mathbf{\Gamma}_y^{1,1}) + B_{33} \times (\mathbf{\Gamma}_x^{1,1} \otimes \mathbf{\Gamma}_y^{0,0});$$

$$\mathbf{K}_\varepsilon^{41} = (\mathbf{K}_\varepsilon^{14})^T; \quad \mathbf{K}_\varepsilon^{42} = (\mathbf{K}_\varepsilon^{24})^T; \quad \mathbf{K}_\varepsilon^{51} = (\mathbf{K}_\varepsilon^{15})^T; \quad \mathbf{K}_\varepsilon^{52} = (\mathbf{K}_\varepsilon^{25})^T;$$

$$\mathbf{K}_\varepsilon^{44} = C_{11} \times (\mathbf{\Gamma}_x^{1,1} \otimes \mathbf{\Gamma}_y^{0,0}) + C_{33} \times (\mathbf{\Gamma}_x^{0,0} \otimes \mathbf{\Gamma}_y^{1,1});$$

$$\mathbf{K}_\varepsilon^{45} = C_{12} \times (\mathbf{\Gamma}_x^{1,0} \otimes \mathbf{\Gamma}_y^{0,1}) + C_{33} \times (\mathbf{\Gamma}_x^{0,1} \otimes \mathbf{\Gamma}_y^{1,0});$$

$$\mathbf{K}_\varepsilon^{54} = (\mathbf{K}_\varepsilon^{45})^T; \quad \mathbf{K}_\varepsilon^{55} = C_{11} \times (\mathbf{\Gamma}_x^{0,0} \otimes \mathbf{\Gamma}_y^{1,1}) + C_{33} \times (\mathbf{\Gamma}_x^{1,1} \otimes \mathbf{\Gamma}_y^{0,0});$$

with

$$\{A_{11}, A_{12}, A_{33}\} = \int_{-h/2}^{h/2} \frac{bE(z)}{1-\mu^2} \{\, 1,\ \mu,\ (1-\mu)/2 \,\} \mathrm{d}z$$

$$\{B_{11}, B_{12}, B_{33}\} = \int_{-h/2}^{h/2} \frac{zbE(z)}{1-\mu^2} \{\, 1,\ \mu,\ (1-\mu)/2 \,\} \mathrm{d}z$$

$$\{C_{11}, C_{12}, C_{33}\} = \int_{-h/2}^{h/2} \frac{z^2 bE(z)}{1-\mu^2} \{\, 1,\ \mu,\ (1-\mu)/2 \,\} \mathrm{d}z$$

where the details of integration matrixes $\mathbf{\Gamma}$ can be found in Appendix.

$$\mathbf{K}_\gamma = \begin{bmatrix} 0 & 0 & 0 & 0 & 0 \\ 0 & 0 & 0 & 0 & 0 \\ 0 & 0 & \mathbf{K}_\gamma^{33} & \mathbf{K}_\gamma^{34} & \mathbf{K}_\gamma^{35} \\ 0 & 0 & \mathbf{K}_\gamma^{43} & \mathbf{K}_\gamma^{44} & 0 \\ 0 & 0 & \mathbf{K}_\gamma^{53} & 0 & \mathbf{K}_\gamma^{55} \end{bmatrix} \tag{35}$$

where

$$\mathbf{K}_{\gamma}^{33} = N \times (\mathbf{\Gamma}_{x}^{1,1} \otimes \mathbf{\Gamma}_{y}^{0,0}) + N \times (\mathbf{\Gamma}_{x}^{0,0} \otimes \mathbf{\Gamma}_{y}^{1,1}); \quad \mathbf{K}_{\gamma}^{34} = -N \times (\mathbf{\Gamma}_{x}^{1,0} \otimes \mathbf{\Gamma}_{y}^{0,0});$$

$$\mathbf{K}_{\gamma}^{35} = -N \times (\mathbf{\Gamma}_{x}^{0,0} \otimes \mathbf{\Gamma}_{y}^{1,0}); \quad \mathbf{K}_{\gamma}^{43} = (\mathbf{K}_{\gamma}^{34})^{T}; \quad \mathbf{K}_{\gamma}^{44} = N \times (\mathbf{\Gamma}_{x}^{0,0} \otimes \mathbf{\Gamma}_{y}^{0,0});$$

$$\mathbf{K}_{\gamma}^{53} = (\mathbf{K}_{\gamma}^{35})^{T}; \quad \mathbf{K}_{\gamma}^{55} = N \times (\mathbf{\Gamma}_{x}^{0,0} \otimes \mathbf{\Gamma}_{y}^{0,0})$$

with $N = \int_{-h/2}^{h/2} \frac{kbE(z)}{2(1+\mu)} \mathrm{d}z$.
The force vector $\boldsymbol{F}$ can be expressed as

$$\boldsymbol{F} = (\mathbf{T})^{T} l_{ex} l_{ey} \int_{0}^{1} \int_{0}^{1} q(\xi, \eta) \mathbf{\Phi}^{T} \mathrm{d}\xi \mathrm{d}\eta \tag{36}$$

where l_{ex} and l_{ey} are the element lengths, respectively, and $q(\xi, \eta)$ is uniform distributed load.

3.3.2 Free vibration analysis of BSWI Mindlin plate

In this section, the free vibration analysis of Mindlin plate is formulated and implemented. According to Hamilton's principle, the equation of motions for free vibration analysis of Mindlin plate can be expressed as

$$\delta\Pi = \int_{t_1}^{t_2} (\delta U - \delta T) \mathrm{d}t = 0 \tag{37}$$

Substituting Eqs. (29-30) into Eq. 37, the basic governing equation of free vibration problem is obtained as

$$(\mathbf{K} - \omega^{2}\mathbf{M})\mathbf{X} = \mathbf{0} \tag{38}$$

where ω is natural frequency and $\mathbf{X}$ is the mode shape of Mindlin plate. The stiffness matrix $\mathbf{K}$ has been obtained in previous section. Similarly, the corresponding mass matrix $\mathbf{M}$ can be obtained as

$$\mathbf{M} = \begin{bmatrix} \mathbf{M}_{11} & 0 & 0 & \mathbf{M}_{14} & 0 \\ 0 & \mathbf{M}_{22} & 0 & 0 & \mathbf{M}_{25} \\ 0 & 0 & \mathbf{M}_{33} & 0 & 0 \\ \mathbf{M}_{41} & 0 & 0 & \mathbf{M}_{44} & 0 \\ 0 & \mathbf{M}_{52} & 0 & 0 & \mathbf{M}_{55} \end{bmatrix} \tag{39}$$

where $\mathbf{M}_{11} = R_{11} \times (\mathbf{\Gamma}_{x}^{0,0} \otimes \mathbf{\Gamma}_{y}^{0,0})$; $\mathbf{M}_{11} = \mathbf{M}_{22} = \mathbf{M}_{33}$; $M_{14} = R_{22} \times (\mathbf{\Gamma}_{x}^{0,0} \otimes \mathbf{\Gamma}_{y}^{0,0})$; $\mathbf{M}_{14} = \mathbf{M}_{25} = \mathbf{M}_{41} = \mathbf{M}_{25}$, $\mathbf{M}_{44} = R_{33} \times (\mathbf{\Gamma}_{x}^{0,0} \otimes \mathbf{\Gamma}_{y}^{0,0})$; $\mathbf{M}_{44} = \mathbf{M}_{55}$

with $\{R_{11}, R_{22}, R_{33}\} = \int_{-h/2}^{h/2} b\rho(z)\{1, -z, z^{2}\} \mathrm{d}z$.

3.3.3 Buckling analysis of BSWI Mindlin plate

In this section, the buckling analysis of Mindlin plate is formulated and implemented. The buckling analysis of Mindlin plate involves the solution of eigenvalue problem

$$(\mathbf{K}-\lambda\mathbf{K}_G)\mathbf{X}=\mathbf{0} \tag{40}$$

where $\mathbf{K}$ is the stiffness matrix, $\mathbf{K}_G$ is the geometric matrix, λ is the critical load and $\mathbf{X}$ is the corresponding buckling mode shape of Mindlin plate. The critical load λ can be obtained by solving Eq. 40. The geometric stiffness matrix $\mathbf{K}_G$ can be written as [Hinton (1988)]

$$\mathbf{K}_G=\int_V G_u^T\sigma^0 g_u^d V+\int_V G_v^T\sigma^0 g_v^d V+\int_V G_w^T\sigma^0 g_w^d V \tag{41}$$

with

$$g_u=\begin{bmatrix}\frac{\partial u}{\partial x} & 0 & 0\\ \frac{\partial u}{\partial y} & 0 & 0\end{bmatrix}\quad g_v=\begin{bmatrix}0 & \frac{\partial v}{\partial x} & 0\\ 0 & \frac{\partial v}{\partial y} & 0\end{bmatrix}\quad g_w=\begin{bmatrix}0 & 0 & \frac{\partial w}{\partial x}\\ 0 & 0 & \frac{\partial w}{\partial y}\end{bmatrix} \tag{42}$$

where $\sigma^0=\begin{bmatrix}\sigma_x^0 & \tau_{xy}^0\\ \tau_{xy}^0 & \sigma_y^0\end{bmatrix}$ indicates the initial stress of Mindlin plate.

Substituting Eq. 26 and Eq. 42 into Eq. 41, the geometric matrix $\mathbf{K}_G$ formulation via BSWI can be obtained

$$\mathbf{K}_G=\left(\sigma_x^0\mathbf{\Gamma}_x^{1,1}\otimes\mathbf{\Gamma}_y^{0,0}+2\tau_{xy}^0\mathbf{\Gamma}_x^{0,1}\otimes\mathbf{\Gamma}_y^{1,0}+\sigma_y^0\mathbf{\Gamma}_x^{0,0}\otimes\mathbf{\Gamma}_y^{1,1}\right)\begin{bmatrix}h & 0 & 0 & 0 & 0\\ 0 & h & 0 & 0 & 0\\ 0 & 0 & h & 0 & 0\\ 0 & 0 & 0 & \frac{h^3}{12} & 0\\ 0 & 0 & 0 & 0 & \frac{h^3}{12}\end{bmatrix} \tag{43}$$

4 Numerical examples and discussion

In this section, various numerical examples and comparisons are presented and discussed to validate the accuracy and reliability of the proposed BSWI method for bending, free vibration and buckling analysis of FG plates. The shear correct factor k is taken as 5/6 for all comparison studies. For convenience, the boundary conditions such as clamped supported, simply supported and free are indicated as C, S and F, respectively. The non-dimensional parameters used in this paper are defined as follows

$$\hat{w}=w\left(\frac{a}{2},\frac{b}{2}\right)/h\quad \bar{w}=\frac{10E_ch^3}{q_0a^4}w\left(\frac{a}{2},\frac{b}{2}\right)\quad w^*=\frac{25E_uh^3}{3q_0a^4(1-\nu^2)}w\left(\frac{a}{2},\frac{b}{2}\right) \tag{44}$$

$$\hat{\omega} = \omega h\sqrt{\rho_c/E_c} \quad \bar{\omega} = \sqrt{\frac{12(1-\nu^2)\rho_c\omega^2a^2b^2}{\pi^4E_ch^2}} \quad \omega^* = \omega a^2\sqrt{\rho_c/E_c}/h \tag{45}$$

$$\hat{\lambda} = \frac{b^2F_{\mathrm{cr}}E_uh^3}{12\pi^2(1-\nu^2)} \quad \bar{\lambda} = \frac{b^2F_{\mathrm{cr}}}{\pi^2E_m} \quad \lambda^* = \frac{a^2F_{\mathrm{cr}}}{E_mh^3} \tag{46}$$

4.1 Bending problem

4.1.1 Accuracy and efficient of BSWI method for bending analysis of FG plate

Example 1: The first comparison study is considered to verify the accuracy and efficient of proposed BSWI method for bending analysis of SSSS FG square plate (a/b = 1). The FG plate is made of aluminum (Al) and zirconia (ZrO_2), and the length-to-thickness ratio is taken as a/h= 5 with volume fraction indexes n= 0, 0.5, 1, 2 and ∞. The Al/ZrO_2 plate is subjected to uniform distributed load. Ferreira [Ferreira et al. (2005)] has given referential solutions for this problem based on the collocation multi-quadric radial basis functions by TSDT. Moreover, Singh [Talha and Singh (2010)] has conducted the convergence of this problem based on HSDT. By aid of one BSWI Mindlin plate element, the calculated non-dimensional deflections $\hat{w}$ are in good agreement with results given by Singh (5×5) [Talha and Singh (2010)] mesh and also almost identical with results given by Ferreira [Ferreira et al. (2005)] shown in Table 2. This example demonstrates that the proposed BSWI method is highly accuracy and efficient for bending analysis of FG plate. It should be noted that the proposed method adopts just one BSWI element. Hence, one BSWI element is adopted in the following examples if no explanation is given.

Table 2: The deflections $\hat{w}$ of SSSS Al/ZrO_2 square plate with various volume fraction indexes (a/h= 5).

Method	volume fraction indexes n				
	0	0.5	1	2	∞
HSDT (2×2)	0.0285	0.0357	0.0394	0.0430	0.0596
HSDT (3×3)	0.0352	0.0439	0.0487	0.0536	0.0738
HSDT (4×4)	0.0269	0.0336	0.0373	0.0409	0.0564
HSDT (5×5)	0.0250	0.0319	0.0358	0.0393	0.0541
TSDT	0.0247	0.0313	0.0351	0.0388	0.0534
Present	0.0248	0.0314	0.0351	0.0386	0.0535

4.1.2 *Effect of volume fraction indexes*

Example 2: Another comparison study is employed to investigate a moderately thick Al/Al_2O_3 square plate (a/h= 10) with various volume fraction indexes. The Al/Al_2O_3 is also subjected to uniform distributed load. The Al/Al_2O_3 plate is fully simply supported (SSSS) and the volume fraction index varies from 0 to ∞. The obtained non-dimensional deflections $\bar{w}$ tabulated in Table 3 are compared with those referential solutions given by Zenkour [Zenkour (2006)] based on the generalized shear deformation theory (GSDT), Thai [Thai and Choi (2013)] based on FSDT. It can be observed that the proposed method achieves an excellent agreement with Thai [Thai and Choi (2013)] for Al/Al_2O_3 plates with all volume fraction indexes. For ceramic rich (n = 0) and metal rich ($n = \infty$), the results are almost identical. However, the other obtained results are slightly small compared with results given by Zenkour [Zenkour (2006)]. These differences may be caused by shear correct factor used in FSDT while this factor is not needed in GSDT. The differences is so slight that the BSWI method still gives satisfactory solutions for Al/Al_2O_3 plates subjected to uniform distributed load. It is also observed that the non-dimensional deflection increases as volume fraction index increases. The full ceramic plate (n = 0) has the maximum bending stiffness and the bending stiffness reduces gradually as volume fraction index increases. The variation of non-dimensional stresses σ_{xx} and τ_{xy} through the thickness of Al/Al_2O_3 plate under uniform distributed load are presented in Fig. 4. The stresses also vary continuously and smoothly throughout the thickness of Al/Al_2O_3 plate which can effectively reduce the influence of interface and eliminate high interfacial stress.

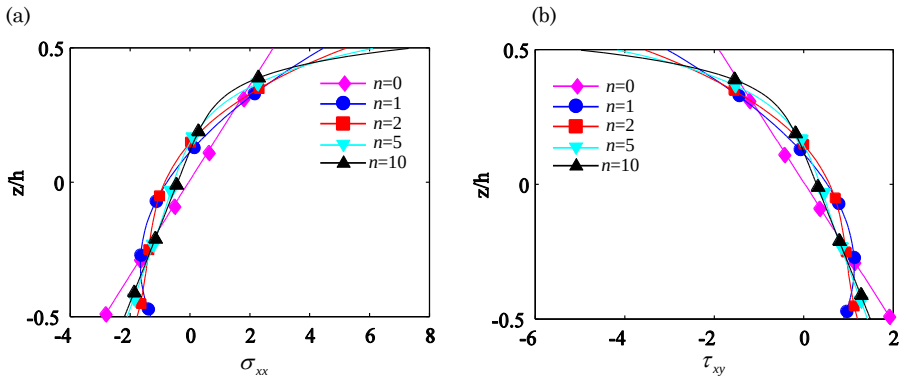

Figure 4: The stresses σ_{xx} and τ_{xy} through the thickness of SSSS Al/Al_2O_3 square plate subjected to uniform distributed load (a/h= 10).

Table 3: The deflections $\bar{w}$ of SSSS Al/ Al_2O_3 square plate subjected to uniform distributed load (a/h= 10).

Method	volume fraction indexes n							
	0	1	2	3	4	5	10	∞
GSDT	0.4665	0.9287	1.1940	1.3200	1.3890	1.4356	1.5876	2.5327
FSDT	0.4666	0.9288	1.1909	1.3123	1.3770	1.4205	1.5697	2.5329
Present	0.4666	0.9288	1.1910	1.3124	1.3770	1.4205	1.5697	2.5330

4.1.3 Effect of length-to-thickness ratios

Example 3: The next comparison study is employed to discuss a Al/Al_2O_3 square plate subjected to sinusoidal distributed load ($q = q_0 \sin(\pi x/a) \times \sin(\pi y/b)$) with different length-to-thickness ratios. The length-to-thickness ratios are chosen as a/h= 4, 10 and 100 for thick plate, moderately thick plate and thin plate. The non-dimensional deflections $\bar{w}$ with volume fraction indexes n = 1, 4 and 10 are calculated and presented in Table 4. The similar problem has been investigated by Carrera [Carrera et al. (2008)] using unified formulation method (UFM), Brischetto [Carrera et al. (2011)] based on HSDT, and Ferreira [Neves et al. (2013)] based on 3D HSDT. These literatures also give solutions based on CPT and FSDT. Compared with other methods, the obtained results are satisfactory especially for thin plate (a/h= 100). With the decreasing of length-to-thickness ratio, the plate becomes thicker while the differences among the Carrera [Carrera et al. (2008)], Brischetto [Carrera et al. (2011)] and Ferreira [Neves et al. (2013)] become obvious, especially for lager volume fraction index. Considering the higher terms, the HSDT method can obtain more accurate results than FSDT for thick plate. The differences between the HSDT and FSDT method become smaller since the effect of transverse shear deformation becomes weak with the increasing length-to-height ratio. Although the HSDT method gives better solutions for thick and thin plate, their equations are much more complicated than those of FSDT. And solutions in Table 4. show that the BSWI element formulated by FSDT could give satisfactory results and it is very effective to investigate behavior of FG plate. Fig. 5. shows the non-dimensional deflections of plates along $y = b/2$ with various volume fraction indexes.

4.1.4 Effect of boundary conditions

Example 4: In addition, a comparison study is presented to investigate a Al/Al_2O_3 square thin plate (a/h= 100) subjected to uniformly distributed load with simply

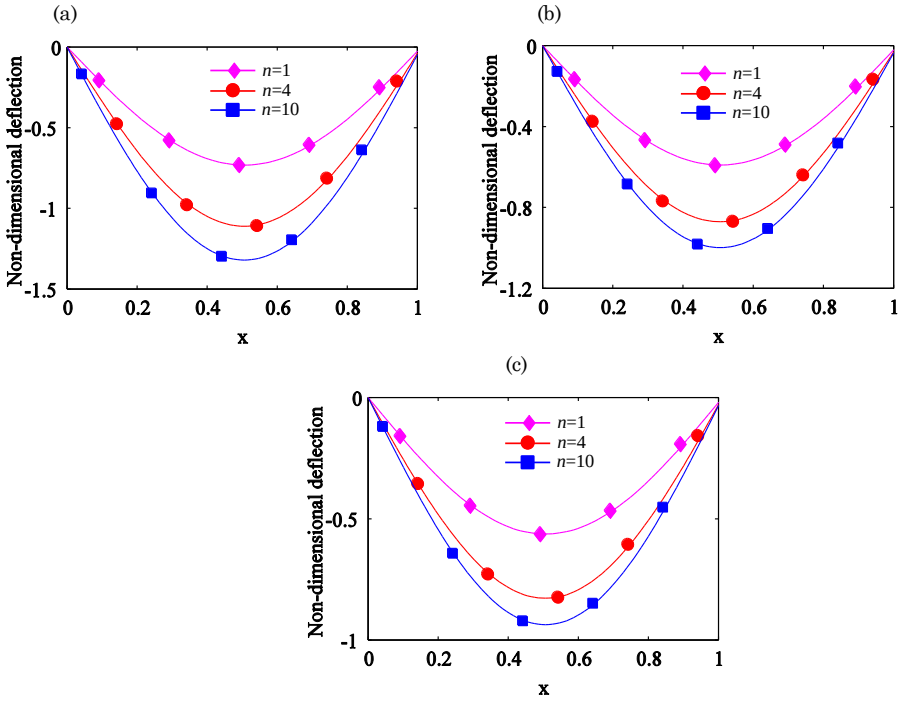

Figure 5: The deformations of Al/Al_2O_3 plates along $y = b/2$ with various volume fraction indexes (a) $a/h = 4$ (b) $a/h = 10$ (c) $a/h = 100$.

Table 4: The deflections $\bar{w}$ of SSSS Al/Al_2O_3 square plate subjected to sinusoidal distributed load.

Method	n=1			n=4			n=10		
	a/h=4	a/h=10	a/h=100	a/h=4	a/h=10	a/h=100	a/h=4	a/h=10	a/h=100
UFM	0.7171	0.5875	0.5625	1.1585	0.8821	0.8286	1.3745	1.0072	0.9361
HSDT	0.7289	0.5890	0.5625	1.1673	0.8828	0.8286	1.3925	1.0090	0.9361
3D HSDT	0.7308	0.5913	0.5648	1.1552	0.8770	0.8241	1.3760	0.9952	0.9228
CPT	0.5623	0.5623	0.5623	0.8281	0.8281	0.8281	0.9354	0.9354	0.9354
FSDT	0.7291	0.5889	0.5625	1.1125	0.8736	0.8280	1.3178	0.9966	0.9360
Present	0.7292	0.5891	0.5625	1.1127	0.8738	0.8285	1.3180	0.9968	0.9359

supported (SSSS) and clamped supported (CCCC). The non-dimensional deflections w^* are tabulated in Table 5 for different volume fraction indexes. The obtained results are compared with those solutions given by Singha [Singha et al. (2011)] based on FSDT. It is clearly that the solutions obtained by the proposed BSWI method get a great agreement with Singha's [Singha et al. (2011)] solutions

for all volume fraction indexes in SSSS and CCCC cases. It is also found that the non-dimensional deflection decreases as the constrain increase. The variations of non-dimensional deflections w^* of Al/Al_2O_3 plates for different length-to-thickness ratios are illustrated in Fig. 6. for SSSS and CCCC cases. In order to clarify the deflections of Al/Al_2O_3 plates, the non-dimensional deflection maps of the whole Al/Al_2O_3 plates with n = 10 are shown in Fig. 7. The solutions of the whole Al/Al_2O_3 plate can be directly observed in Fig. 7.

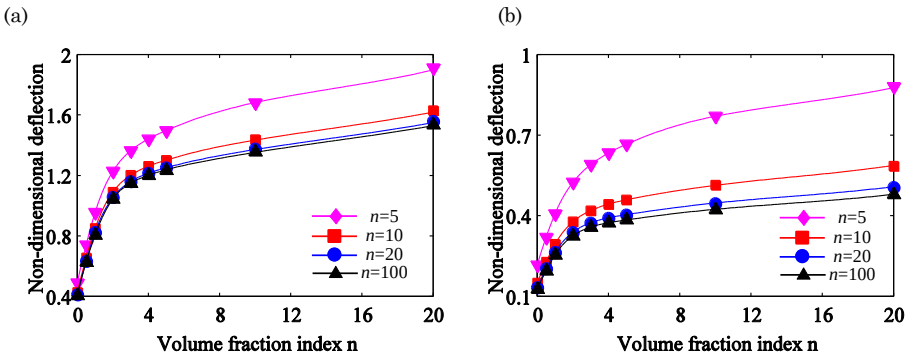

Figure 6: The deflections $w*$ of Al/Al_2O_3 plates for different length-to-thickness ratios (a) SSSS (b) CCCC.

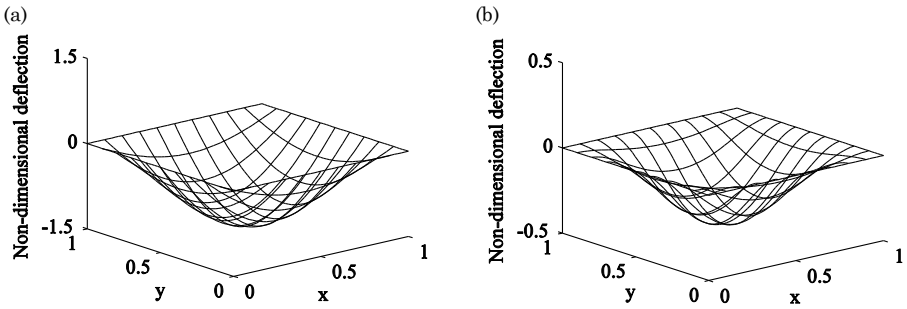

Figure 7: The deflection maps of the whole Al/Al_2O_3 plates with n = 10 (a) SSSS (b) CCCC.

Table 5: The deflections w^* of SSSS and CCCC square Al/Al_2O_3 plate subjected to uniformly distributed load (a/h= 100).

n	0	0.5	1	2	3	4	5	10	20	∞
SSSS										
FSDT	0.4064	0.6269	0.8154	1.0449	1.1482	1.2011	1.2359	1.3569	1.5362	2.2064
Present	0.4066	0.6272	0.8159	1.0455	1.1487	1.2016	1.2362	1.3572	1.5368	2.2076
CCCC										
FSDT	0.1267	0.1955	0.2542	0.3258	0.3580	0.3746	0.3854	0.4233	0.4792	0.6881
Present	0.1269	0.1957	0.2546	0.3262	0.3584	0.3749	0.3857	0.4235	0.4795	0.6887

4.2 Free vibration problem

4.2.1 Accuracy and efficient of BSWI method for free vibration analysis of FG plate

Example 5: Firstly, a comparison study is employed to verify the accuracy and efficient of the proposed BSWI method for free vibration analysis of Al/Al_2O_3 square plate. The length-to-thickness ratios are taken as a/h= 5 and 10 and volume fraction indexes are chosen as n= 0, 0.5, 1, 4, 10. The fundamental non-dimensional frequency parameters $\hat{\omega}$ obtained using the BSWI element are compared with element-free kp-Ritz method solutions of Liew [Zhao et al. (2009a)], the FSDT solutions of Thai [Thai and Choi (2013)] and Hashemi [Hosseini-Hashemi et al. (2010)] in Table 6 for SSSS case. Obviously, the solutions given by the proposed BSWI method are in excellent agreement with the referential solutions given by Liew [Zhao et al. (2009a)], Thai [Thai and Choi (2013)] and Hashemi [Hosseini-Hashemi et al. (2010)], especially for moderately thick ones (a/h = 10). This comparison study shows that the accuracy and efficiency of the present method are valid and effective for free vibration analysis of FG plates.

Example 6: Another comparison study is considered to validate the accuracy and efficiency of proposed BSWI method for square FG plate with different boundary conditions (BCS). In this study, the length-to-thickness ratio of square Al/ZrO_2 plate is taken as a/h= 5. The Al/ZrO_2 plate material properties are assumed to vary continuously throughout the thickness of plate with volume fraction index n = 5. The non-dimensional frequency parameters $\bar{\omega}$ are calculated and shown in Table 7 for SSSS, CCCC and SCSC cases. The comparison results have also been given by Singh [Talha and Singh (2010)] based on HSDT and Aydogdu [Uymaz and Aydogdu (2007)] based on small strain linear elasticity theory. It is obviously that the BSWI method achieves a high accuracy compared with Aydogdu [Uymaz and Aydogdu (2007)]. Due to excellent characteristics of BSWI, the proposed BSWI

method with adopting just one BSWI element can get excellent results for various boundary conditions.

Table 6: The frequency parameters $\hat{\omega}$ of SSSS square Al/Al_2O_3 plate.

a/*h*	Method	volume fraction indexes *n*				
		0	0.5	1	4	10
5	Liew (9×9)	0.2018	0.1726	0.1559	0.1332	0.1261
	Liew (13×13)	0.2045	0.1748	0.1579	0.1349	0.1277
	Liew (17×17)	0.2055	0.1757	0.1587	0.1356	0.1284
	Thai	0.2112	0.1805	0.1631	0.1397	0.1324
	Hashemi	0.2112	0.1806	0.1650	0.1371	0.1304
	Present	0.2112	0.1804	0.1630	0.1396	0.1323
10	Liew (9×9)	0.0561	0.0476	0.0430	0.0371	0.0355
	Liew (13×13)	0.0565	0.0480	0.0433	0.0374	0.0358
	Liew (17×17)	0.0567	0.0482	0.0435	0.0376	0.0359
	Thai	0.0577	0.0490	0.0442	0.0382	0.0366
	Hashemi	0.0578	0.0492	0.0445	0.0383	0.0363
	Present	0.0577	0.0490	0.0442	0.0382	0.0366

Table 7: The frequency parameters $\bar{\omega}$ of Al/ZrO_2 square plate for various boundary conditions (*a*/*h*=5, *n*=5).

Method	BCS		
	SSSS	CCCC	SCSC
Singh (3×3)	1.4321	2.2669	2.0260
Singh (4×4)	1.4222	2.1944	1.9287
Singh (5×5)	1.4165	2.1540	1.8161
Aydogdu	1.4106	2.1447	1.8055
Present	1.4102	2.1429	1.7990

4.2.2 Effect of the thickness-to-width ratios

Example 7: The influence of thickness-to-width ratios on the free vibration of Al/Al_2O_3 plate is considered in this comparison. The aim of this example is to verify the obtained results with the SSDT solutions of Thai [Thai and Vo (2013)], the Reddy's TSDT solutions of Hashemi [Hosseini-Hashemi et al. (2011b)] and

HSDT solutions of Matsunaga [Matsunaga (2008)]. The square Al/Al_2O_3 plate is full simply support (SSSS) and the first three non-dimensional frequency parameters $\hat{\omega}$ for a/h= 5, 10 and fundamental non-dimensional frequency parameters $\hat{\omega}$ for a/h= 20 with volume fraction indexes varying from 0 to ∞ are tabulated in Table 8. It can be observed that the results obtained by present BSWI method are good in agreement with almost solutions of Thai [Thai and Vo (2013)], Hashemi [Hosseini-Hashemi et al. (2011b)] and Matsunaga [Matsunaga (2008)], especially for moderately plate (a/h = 10) or thin plate (a/h = 20). This example verifies the proposed BSWI method has an excellent accuracy for free vibration problem of Al/Al_2O_3 plates. It is also found that the non-dimensional frequency parameter decreases as the volume fraction index increases. This phenomenon may be caused by larger volume fraction index leads to metal rich of Al/Al_2O_3 plate which will result in decrease of stiffness. In order to verify the correctness of the proposed BSWI method, the fist six mode shapes of SSSS square Al/Al_2O_3 plates with a/h = 10 and n = 10 are shown in Fig. 8. It is observed that the solving mode shapes are very consistent with the real vibration of square plate which verifies the correctness of the proposed BSWI method once more.

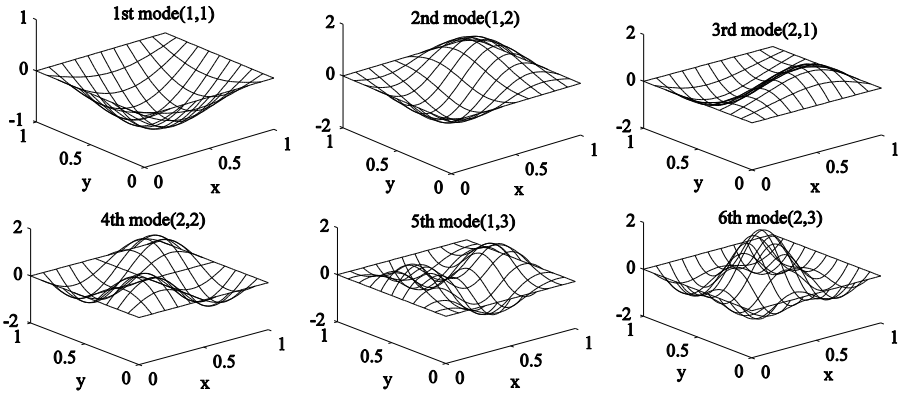

Figure 8: The first six mode shapes of SSSS square Al/Al_2O_3 plates (a/h =10 and n =10).

Example 8: The next example is considered for Al/Al_2O_3 rectangular plate with different thickness-to-width ratios. The other corresponding parameters are the same with the example 7. The first four non-dimensional frequency parameters $\tilde{\omega}$ of Al/Al_2O_3 rectangular plate (b/a = 2) are calculated and shown in Table 9. The comparison solutions are given by Choi [Thai et al. (2013)] based on an efficient shear deformation theory and Hashemi [Hosseini-Hashemi et al. (2011a)] based on the Reissner-Mindlin plate theory (FSDT). A good agreement between the ref-

Table 8: The frequency parameters $\hat{\omega}$ of SSSS square Al/Al_2O_3 plate.

a/*h*	(*m*,*n*)	Method	volume fraction indexes *n*					
			0	0.5	1	4	10	∞
5	(1,1)	TSDT	0.2113	0.1807	0.1631	0.1378	0.1301	0.1076
		HSDT	0.2121	0.1819	0.1640	0.1383	0.1306	0.1077
		SSDT	0.2112	0.1805	0.1631	0.1397	0.1324	0.1076
		Present	0.2112	0.1802	0.1625	0.1384	0.1315	0.1075
	(1,2)	TSDT	0.4623	0.3989	0.3607	0.2980	0.2771	0.2355
		HSDT	0.4658	0.4040	0.3644	0.3000	0.2790	0.2365
		SSDT	0.4618	0.3978	0.3604	0.3049	0.2856	0.2352
		Present	0.4618	0.3986	0.3625	0.3107	0.2865	0.2351
	(2,2)	TSDT	0.6688	0.5803	0.5254	0.4284	0.3948	0.3404
		HSDT	0.6753	0.5891	0.5444	0.4362	0.3981	0.3429
		SSDT	0.6676	0.5779	0.5245	0.4405	0.4097	0.3399
		Present	0.6676	0.5779	0.5248	0.4401	0.4090	0.3398
10	(1,1)	TSDT	0.0577	0.0490	0.0442	0.0381	0.0364	0.0293
		HSDT	0.0578	0.0492	0.0443	0.0381	0.0364	0.0293
		SSDT	0.0577	0.0490	0.0442	0.0382	0.0366	0.0293
		Present	0.0577	0.0491	0.0443	0.0384	0.0367	0.0294
	(1,2)	TSDT	0.1377	0.1174	0.1059	0.0903	0.0856	0.0701
		HSDT	0.1381	0.1180	0.1063	0.0904	0.0859	0.0701
		SSDT	0.1376	0.1173	0.1059	0.0911	0.0867	0.0701
		Present	0.1376	0.1171	0.1055	0.0903	0.0864	0.0701
	(2,2)	TSDT	0.2113	0.1807	0.1631	0.1378	0.1301	0.1076
		HSDT	0.2121	0.1819	0.1640	0.1383	0.1306	0.1077
		SSDT	0.2112	0.1805	0.1631	0.1397	0.1324	0.1076
		Present	0.2112	0.1808	0.1638	0.1405	0.1327	0.1075
20	(1,1)	TSDT	0.0148	0.0125	0.0113	0.0098	0.0094	-
		SSDT	0.0148	0.0125	0.0113	0.0098	0.0094	-
		Present	0.0148	0.0126	0.0114	0.0099	0.0095	0.0075

erential solutions and results obtained by proposed BSWI method is observed for almost all the vibration mode shapes of Al/Al_2O_3 plates. However, the differences between the results for the forth vibration modes of thick plate (a/h = 5) increase slightly with the increase of volume fraction indexes. These differences may be caused by the fewer degrees of freedom used in BSWI for estimating frequencies. The fist six mode shapes of SSSS Al/Al_2O_3 rectangular plates with a/h =10 and n =10 are shown in Fig. 9. These mode shapes are also very consistent with the real vibration of rectangular plate which verifies the correctness of the proposed BSWI method once more. So the proposed BSWI method is not only suitable for solving the free vibration problem of Al/Al_2O_3 square plate but also for those of Al/Al_2O_3 rectangular plate.

Table 9: The frequency parameters ω^* of SSSS rectangular Al/Al_2O_3 plate (b/a = 2).

a/h	Mode	Method	volume fraction indexes n						
			0	0.5	1	2	5	8	10
5	(1,1)	Choi	3.4412	2.9347	2.6475	2.3949	2.2272	2.1697	2.1407
		Hashemi	3.4409	2.9322	2.6473	2.4017	2.2528	2.1985	2.1677
		Present	3.4409	2.9315	2.6462	2.4003	2.2510	2.1967	2.1658
	(1,2)	Choi	5.2813	4.5180	4.0781	3.6805	3.3938	3.2964	3.2514
		Hashemi	5.2802	4.5122	4.0773	3.6953	3.4492	3.3587	3.3094
		Present	5.2803	4.5111	4.0757	3.6931	3.4465	3.3558	3.3066
	(1,3)	Choi	8.0749	6.9366	6.2663	5.6390	5.1425	4.9758	4.9055
		Hashemi	8.0710	6.9231	6.2636	5.6695	5.2579	5.1045	5.0253
		Present	8.0733	6.9233	6.2628	5.6675	5.2547	5.1012	5.0219
	(2,1)	Choi	10.1164	8.7138	7.8762	7.0751	6.4074	6.1846	6.0954
		Hashemi	9.7416	8.6926	7.8711	7.1189	6.5749	5.9062	5.7518
		Present	10.1091	8.6905	7.8681	7.1150	6.5699	6.3656	6.2631
10	(1,1)	Choi	3.6518	3.0990	2.7937	2.5364	2.3916	2.3411	2.3110
		Hashemi	3.6518	3.0983	2.7937	2.5386	2.3998	2.3504	2.3197
		Present	3.6518	3.0976	2.7926	2.5372	2.3980	2.3485	2.3178
	(1,2)	Choi	5.7694	4.9014	4.4192	4.0090	3.7682	3.6846	3.6368
		Hashemi	5.7693	4.8997	4.4192	4.0142	3.7881	3.7072	3.6580
		Present	5.7697	4.8988	4.4177	4.0123	3.7855	3.7044	3.6552
	(1,3)	Choi	9.1880	7.8189	7.0515	6.3886	5.9765	5.8341	5.7575
		Hashemi	9.1876	7.8145	7.0512	6.4015	6.0247	5.8887	5.8086
		Present	9.1957	7.8201	7.0556	6.4043	6.0253	5.8886	5.8083
	(2,1)	Choi	11.8315	10.0810	9.0933	8.2309	7.6731	7.4813	7.3821
		Hashemi	11.8310	10.0740	9.0928	8.2515	7.7505	7.5688	7.4639
		Present	11.8313	10.0719	9.0903	8.2483	7.7457	7.5635	7.4584
20	(1,1)	Choi	3.7123	3.1458	2.8352	2.5771	2.4403	2.3923	2.3619
		Hashemi	3.7123	3.1456	2.8352	2.5777	2.4425	2.3948	2.3642
		Present	3.7123	3.1451	2.8342	2.5763	2.4407	2.3929	2.3623
	(1,2)	Choi	5.9199	5.0180	4.5228	4.1100	3.8884	3.8107	3.7622
		Hashemi	5.9198	5.0175	4.5228	4.1115	3.8939	3.8170	3.7681
		Present	5.9211	5.0174	4.5222	4.1103	3.8919	3.8148	3.7658
	(1,3)	Choi	9.5669	8.1133	7.3132	6.6433	6.2760	6.1476	6.0690
		Hashemi	9.5669	8.1121	7.3132	6.6471	6.2903	6.1639	6.0843
		Present	9.5963	8.1380	7.3368	6.6671	6.3046	6.1760	6.0957
	(2,1)	Choi	12.4562	10.5677	9.5261	8.6509	8.1636	7.9934	7.8909
		Hashemi	12.456	10.566	9.5261	8.6572	8.1875	8.0207	7.9166
		Present	12.4586	10.5654	9.5244	8.6547	8.1831	8.0158	7.9114

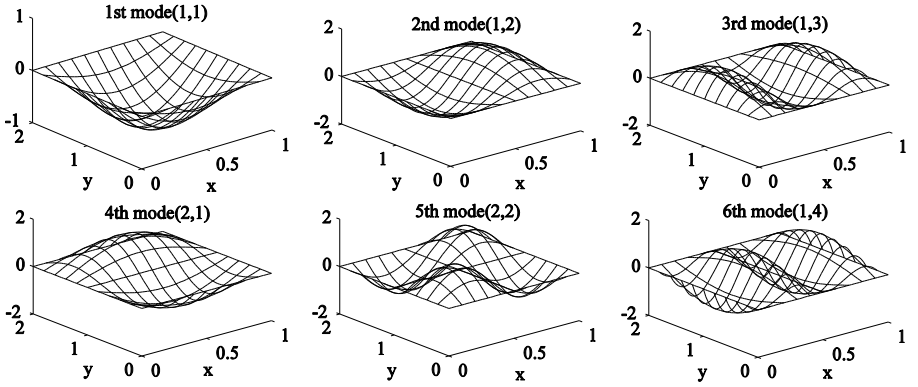

Figure 9: The first six mode shapes of SSSS rectangular Al/Al_2O_3 plates (a/h =10 and n =10).

4.2.3 Effect of boundary conditions

Example 9: The boundary conditions also play a very important role in estimating the frequencies of Al/Al_2O_3 plate. Hence, the following example is employed to verify the validity of proposed BSWI method for free vibration analysis of Al/Al_2O_3 square plate with different boundary conditions. The fundamental non-dimensional frequency parameters ω^* for thickness-to-width ratios a/h= 5, 10 with SSSS, CCCC, CFFF, SCSC boundary conditions are calculated and presented in Table 10. The identical problem has been discussed by Liew [Zhu and Liew (2011); Zhao et al. (2009a)] using the local Kriging meshless method and element-free *kp*-Ritz method, and Hashemi [Hosseini-Hashemi et al. (2011a)] using FSDT. Compared with those referential solutions, the proposed BSWI method gives satisfactory solutions for different boundary conditions. The variations of non-dimensional frequency parameters ω^* with volume fraction indexes are illustrated in Fig. 10. for SSSS, CCCC, CFFF, SCSC boundary conditions. The constraints of boundary conditions affect stiffness. So the non-dimensional frequency parameter is higher in CCCC cases than other cases. This comparison shows that the formulated FGM BSWI element is very suitable for analyzing free vibration of FG plate with various boundary conditions.

4.3 Buckling problem

4.3.1 Accuracy and stability of BSWI method for buckling analysis of FG plate

Example 10: The first comparison study is employed to verify the accuracy and stability of BSWI method for buckling analysis of FG plate. Since the exact buckling

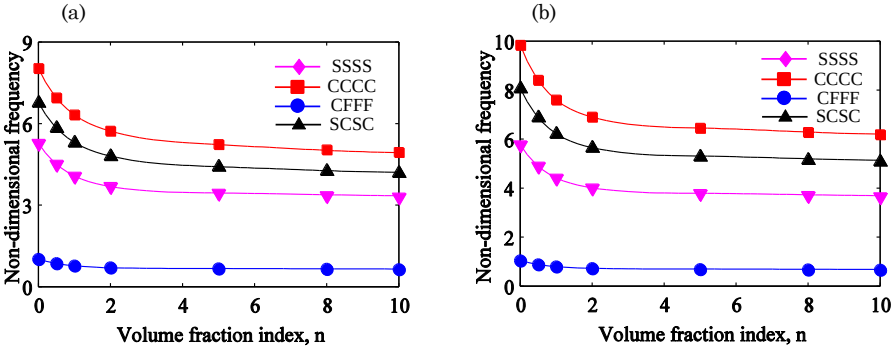

Figure 10: The frequency parameters ω^* of square Al/Al_2O_3 plates with volume fraction index (a) a/h = 5 (b) a/h= 10.

solutions of FG plate are not available in literatures, a homogenous material plate is used here for verification. The homogenous material plate represents a special FG plate with volume fraction index n = 0 or ∞. The thin plate (a/h= 100) subjected to uniaxial compression with SSSS and CCCC cases is considered in this example. The exact buckling factors $\hat{\lambda}$ have been given by Timoshenko [Timoshenko and Gere (2012)] and other referential results have also been given by Cheung [Cheung et al. (2000)], Aliabadi [Purbolaksono and Aliabadi (2005)], Liew [Liew and Chen (2004)], Civalek [Ersoy et al. (2009)] and Xuan [Nguyen-Xuan et al. (2010)]. The obtained results listed in Table 11 has an excellent agreement with the exact solution given by Timoshenko [Timoshenko and Gere (2012)] in SSSS case compared with other methods. Although Cheung's method seems to show a better agreement with exact solutions for CCCC case, the proposed BSWI method also still performances well. This comparison study validates the accuracy of the proposed BSWI method for buckling analysis of FG plate.

4.3.2 A FG square plate subjected to uniaxial compression

Example 11: The buckling factors $\bar{\lambda}$ of FG square plate subjected to uniaxial compression with SSSS boundary condition are considered in this comparison. The FG plate consists of SUS304 and Si_3N_4. The buckling factors are calculated and presented in Table 12. And the present results are compared with the referential solutions given by Tzou [Chen et al. (2009)] based on HSDT with thickness-to-width ratios a/h= 10, 20, 100. Compared with the referential solutions, the present method obtains excellent solutions for different thickness-to-width ratios. Fig. 11. presents the contour plots of the first six buckling mode shapes of square SUS304/Si_3N_4 plate subjected to uniaxial compression on x axis (a/h= 100, n = 10). Obviously,

Table 10: The frequency parameters ω^* of square Al/Al_2O_3 plates with different boundary conditions.

a/h	BCS	volume fraction indexes *n*							
		0	0.5	1	2	5	8	10	10000
5	SSSS	5.2791[a]	4.5101	4.0746	3.6923	3.4461	3.3555	3.3062	2.6857
		5.2802[d]	4.5110	4.0756	3.6930	3.4464	3.3557	3.3065	2.6851
	CCCC	8.0374[a]	6.9609	6.3314	5.7332	5.2395	5.0429	4.9501	4.0887
		8.0267[d]	6.9526	6.3246	5.7280	5.2363	5.0405	4.9480	4.0855
	CFFF	1.0106[a]	0.8580	0.7738	0.7028	0.6631	0.6489	0.6403	0.5142
		1.0106[d]	0.8584	0.7742	0.7033	0.6636	0.6494	0.6408	0.5144
	SCSC	6.7722[a]	5.8451	5.3069	4.8052	4.4133	4.2605	4.1864	3.4451
		6.7663[c]	5.8409	5.3039	4.8032	4.4127	4.2604	4.1865	-
		6.7663[d]	5.8395	5.3018	4.8005	4.4094	4.2569	4.1830	3.4440
10	SSSS	5.7619[a]	4.8914	4.4106	4.0059	3.7806	3.7001	3.6510	2.9313
		5.6763[b]	4.8209	4.3474	3.9474	3.7218	3.6410	3.5923	-
		5.7693[d]	4.8985	4.4174	4.0120	3.7853	3.7043	3.6550	2.9365
	CCCC	9.8710[a]	8.4344	7.6280	6.9233	6.4667	6.2934	6.1988	5.0215
		9.6329[b]	8.2388	7.4533	6.7629	6.3060	6.1314	6.0375	-
		9.8429[d]	8.4107	7.6069	6.9055	6.4533	6.2817	6.1876	5.0099
	CFFF	1.0361[a]	0.8777	0.7910	0.7190	0.6811	0.6677	0.6591	0.5272
		1.0298[b]	0.8728	0.7867	0.7150	0.6768	0.6633	0.6547	-
		1.0382[d]	0.8801	0.7935	0.7213	0.6829	0.6694	0.6608	0.5285
	SCSC	8.0849[a]	6.8964	6.2321	5.6574	5.2987	5.1642	5.0889	4.1129
		8.0702[c]	6.8847	6.2222	5.6494	5.2930	5.1594	5.0844	-
		8.0705[d]	6.8834	6.2201	5.6466	5.2894	5.1555	5.0805	4.1078
a solutions presented by Liew [Zhu and Liew (2011)] using local Kriging meshless method.									
b solutions presented by Liew [Zhao et al. (2009a)] using element-free *kp*-Ritz method.									
c solutions presented by Hosseini-Hashemi [Hosseini-Hashemi et al. (2011a)] based on FSDT.									
d solutions presented using BSWI method.									

Table 11: The buckling factors $\hat{\lambda}$ of square FG plate subjected to uniaxial compression (a/h= 100, n = 0).

BCS	Cheung[54]	FEM[55]	Liew[56]	DSC[57]	DSG3[58]	ES-DSG3[58]	Exact[53]	Present
SSSS	4.002	4.011	4.017	4.011	4.1590	4.0170	4.00	3.9982
CCCC	10.075	10.392	10.308	10.310	11.0446	10.2106	10.07	10.1842

more wrinkles may arise on x axis with the increase of mode shape. The compression load is mainly subjected on x axial, so the plates are most likely to lose stability in x axial direction.

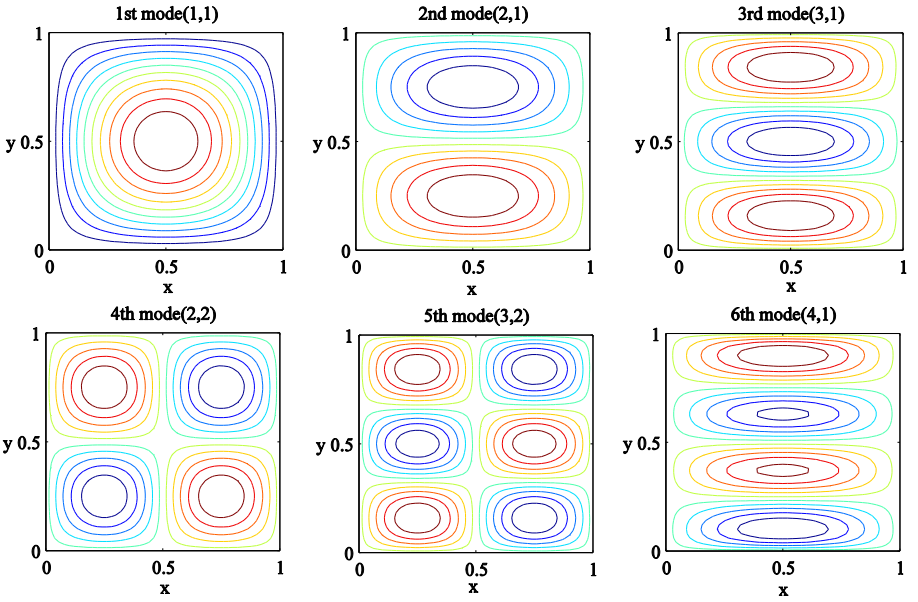

Figure 11: The contour plots of the first six buckling mode shapes of square SUS304/Si_3N_4 plate subjected to uniaxial compression on x axis (a/h= 100, n = 10).

Table 12: The buckling factors $\bar{\lambda}$ of SSSS square SUS304/Si_3N_4 plate subjected to uniaxial compression.

a/h	Method	volume fraction indexes n							
		0	0.1	0.5	1	2	5	10	∞
10	HSDT	0.5148	0.4957	0.4525	0.4299	0.4115	0.3907	0.3753	0.3426
	Present	0.5140	0.4942	0.4484	0.4247	0.4079	0.3918	0.3784	0.3454
20	HSDT	0.5396	0.5194	0.4743	0.4512	0.4329	0.4118	0.3955	0.3600
	Present	0.5396	0.5188	0.4709	0.4465	0.4296	0.4134	0.3994	0.3640
100	HSDT	0.5482	0.5276	0.4818	0.4585	0.4403	0.4192	0.4026	0.3660
	Present	0.5485	0.5274	0.4788	0.4546	0.4374	0.4209	0.4067	0.3702

Example 12: The thin Al/SiC plate (a/h = 100) with SCSC, SSSC, SSSS, SCSF, SSSF, SFSF cases are employed to verify the accuracy and applicability of proposed BSWI method for buckling analysis of Al/SiC square plate subjected to uniaxial compression. Table 13 presents the comparisons of BSWI method with Levy-type solutions based on HSDT. It can be seen that the obtained results are found to be in excellent agreement with Levy-type solutions given by Saidi [Bodaghi and

Saidi (2010)] for different boundary conditions. The variations of non-dimensional buckling factors λ^* of Al/SiC plates subjected to uniaxial compression with volume fraction indexes are illustrated in Fig. 12. for SCSC, SSSC, SSSS, SCSF, SSSF, SFSF cases. It can be observed that the critical buckling factor decreases as the volume fraction index increases. However, the influence of volume fraction index becomes weaker as the volume fraction index increases. This is due to the fact that the larger volume fraction index may lead to metal rich. The constraint of boundary conditions directly affects the buckling load of Al/SiC plates. Thus, the boundary conditions play a very important role for buckling analysis of FG plates. It is meaningful to investigate the buckling analysis of FG plates with different boundary conditions which can be used to guide the practical engineering design.

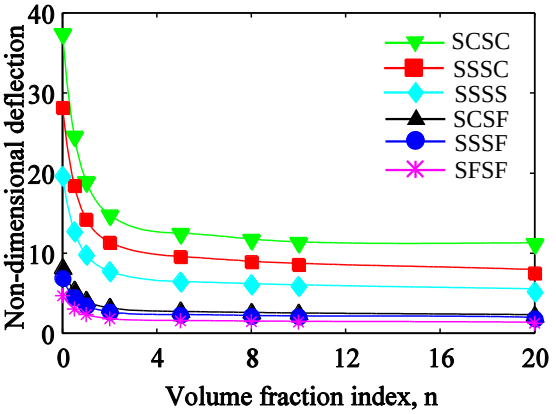

Figure 12: The buckling factors λ^* of SiC plates subjected uniaxial compression with volume fraction indexes (a/h = 100).

4.3.3 A FG square plate subjected to biaxial compression

Example 13: Another comparison of SSSS square Al/Al_2O_3 plate subjected to biaxial compression is considered. Table 14 lists the buckling factors λ^* of Al/Al_2O_3 plate with thickness-to-width ratios a/h= 10, 20, 100. The obtained results are compared with similar solutions given by Choi [Thai et al. (2013)] based on the refined theory of Shimpi. It is observed that the present BSWI method gives satisfactory solutions compared with referential solutions given by Choi [Thai et al. (2013)]. These results get closer with the increase of a/h. The difference may be caused by the influence of transverse shear deformation. The first six buckling modes of SSSS square Al/Al_2O_3 plate subjected to biaxial compression with a/h= 100 and

Table 13: The buckling factors λ^* of square Al/SiC plate subjected to uniaxial compression with different boundary conditions (a/h = 100).

n	Method	BCS					
		SCSC	SSSC	SSSS	SCSF	SSSF	SFSF
0	HSDT	37.7364	28.1637	19.6255	8.1078	6.8767	4.6724
	Present	37.8846	28.1537	19.6131	8.1045	6.8748	4.6781
1	HSDT	18.8094	14.0380	9.7821	4.0412	3.4277	2.3288
	Present	18.9122	14.0402	9.7825	4.0399	3.4164	2.3262
2	HSDT	14.6772	10.9540	7.6331	3.1534	2.6747	1.8172
	Present	14.7517	10.9539	7.7333	3.1515	2.6748	1.8158

Table 14: The buckling factors λ^* of SSSS square Al/Al_2O_3 plate subjected to biaxial compression.

a/h	Method	volume fraction indexes n							
		0	0.5	1	2	5	10	20	100
10	Choi	9.2893	6.0615	4.6696	3.6315	3.0177	2.7264	2.4173	1.9099
	Present	9.1539	5.9889	4.6406	3.6386	3.0408	2.7366	2.4056	1.8837
20	Choi	9.6764	6.2834	4.8337	3.7686	3.1724	2.8834	2.5494	1.9961
	Present	9.6380	6.2555	4.8114	3.7522	3.1654	2.8792	2.5433	1.9885
100	Choi	9.8073	6.3579	4.8888	3.8147	3.2254	2.9376	2.5948	2.0254
	Present	9.8067	6.3587	4.8892	3.8153	3.2277	2.9383	2.5949	2.0254

n = 10 are identical with vibration mode shapes of SSSS square Al/Al_2O_3. Obviously, the wrinkles may arise on x axis or y axis with the increase of mode shape. The compression load is mainly subjected on x axial and y axial at the same time, so the plates may lose stability in x or y axial direction with the same probability.

Example 14: Table 15 presents the buckling factors λ^* of a square Al/SiC FG plate (a/h = 100) subjected to biaxial compression for SCSC, SSSC, SSSS, SCSF, SSSF, SFSF cases. Saidi [Bodaghi and Saidi (2010)] has also given the similar solutions for this problem. The present solutions show a good approximation with the results given by Saidi [Bodaghi and Saidi (2010)]. The variations of non-dimensional buckling factors λ^* of SiC plates subjected to biaxial compression with volume fraction indexes are illustrated in Fig. 13. for SCSC, SSSC, SSSS, SCSF, SSSF, SFSF cases. The similar phenomenon has been explained in example 12. The buckling factors subjected to biaxial compression are smaller than those subjected to uniaxial compression.

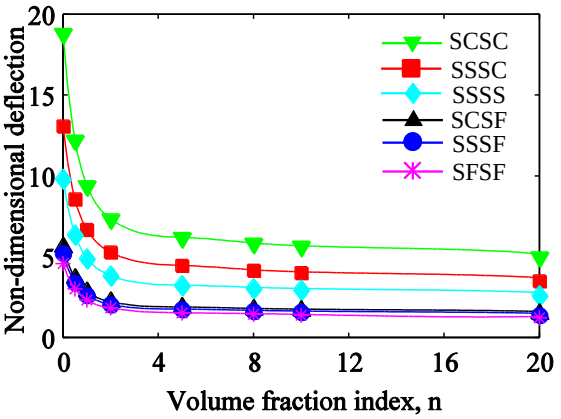

Figure 13: The buckling factors λ^* of Al/SiC plates subjected to biaxial compression with volume fraction indexes (a/h = 100).

Table 15: The buckling factors λ^* of square Al/SiC plate subjected to biaxial compression with different boundary conditions (a/h = 100).

n	Method	BCS					
		SCSC	SSSC	SSSS	SCSF	SSSF	SFSF
0	Saidi	18.7910	13.0643	9.8127	5.6107	5.1768	4.5737
	Present	18.8044	13.0564	9.8067	5.6057	5.1726	4.5714
1	Saidi	9.3661	6.5117	4.8911	2.7965	2.5804	2.4455
	Present	9.3847	6.5098	4.8892	2.7825	2.5846	2.3083
2	Saidi	7.3086	5.0812	3.8165	2.1822	2.0135	1.7788
	Present	7.3330	5.0786	3.8153	2.1741	2.0116	1.7926

5 Conclusion

The objective of this paper is to present an accurate and effective numerical method for the comprehensive study of bending, free vibration and buckling analysis of FG plates. For this purpose, a wavelet finite element, which employs scaling functions of two-dimensional tensor product BSWI as shape functions, is proposed for theoretical analysis of FG plates. The governing motion equations are derived by using the Mindlin plate theory and Hamilton's principle. Then two-dimensional FGM BSWI element is formulated for bending, free vibration and buckling analysis of FG plates. Different numerical examples concerning various length-to-thickness ratios, volume fraction indexes, aspect ratios and boundary conditions are provided

to validate the accuracy, efficiency and the reliability of FGM BSWI element compared with available analytical and numerical solutions in literatures. Satisfactory solutions for bending, free vibration and buckling analysis of FG plates can be achieved using fewer degrees of freedoms. These excellent solutions can be attributed to the excellent characteristics of BSWI. This paper reveals that the proposed wavelet based BSWI finite element method is an efficient numerical tool for the bending, free vibration and buckling problems of FGM structures. What's more, the proposed wavelet-based BSWI finite element method will be promising to be an effective and accurate tool for analyses of FGM structures.

Acknowledgement: This work was supported by the National Natural Science Foundation of China (Nos. 51405369 and 51421004), the China Postdoctoral Science Foundation (No. 2014M560766), and the Fundamental Research Funds for the Central Universities (No. xjj2014107).

References

Abrate, S. (2008): Functionally graded plates behave like homogeneous plates. *Composites part B: engineering,* vol. 39, pp. 151-158.

Akgoz, B.; Civalek, O. (2013a): Buckling analysis of functionally graded microbeams based on the strain gradient theory. *Acta Mechanica,* vol. 224, pp. 2185-2201.

Akgoz, B.; Civalek, O. (2013b): A size-dependent shear deformation beam model based on the strain gradient elasticity theory. *International Journal of Engineering Science,* vol. 70, pp. 1-14.

Ameur, M.; Tounsi, A.; Mechab, I.; El Bedia, A. A. (2011): A new trigonometric shear deformation theory for bending analysis of functionally graded plates resting on elastic foundations. *KSCE Journal of Civil Engineering,* vol. 15, pp. 1405-1414.

Atluri, S.; Sladek, J.; Sladek, V.; Zhu, T. (2000): The local boundary integral equation (LBIE) and it's meshless implementation for linear elasticity. *Computational mechanics,* vol. 25, pp. 180-198.

Atluri, S.; Zhu, T. (1998): A new meshless local Petrov-Galerkin (MLPG) approach in computational mechanics. *Computational mechanics,* vol. 22, pp. 117-127.

Atmane, H. A.; Tounsi, A.; Mechab, I. (2010): Free vibration analysis of functionally graded plates resting on Winkler–Pasternak elastic foundations using a new shear deformation theory. *International Journal of Mechanics and Materials in Design,* vol. 6, pp. 113-121.

Baferani, A. H.; Saidi, A.; Jomehzadeh, E. (2011): An exact solution for free vibration of thin functionally graded rectangular plates. *Proceedings of the Institution of Mechanical Engineers, Part C: Journal of Mechanical Engineering Science,* vol. 225, pp. 526-536.

Benyoucef, S.; Mechab, I.; Tounsi, A.; Fekrar, A.; Atmane, H. A. (2010): Bending of thick functionally graded plates resting on Winkler–Pasternak elastic foundations. *Mechanics of Composite Materials,* vol. 46, pp. 425-434.

Bodaghi, M.; Saidi, A. (2010): Levy-type solution for buckling analysis of thick functionally graded rectangular plates based on the higher-order shear deformation plate theory. *Applied Mathematical Modelling,* vol. 34, pp. 3659-3673.

Carrera, E.; Brischetto, S.; Cinefra, M.; Soave, M. (2011): Effects of thickness stretching in functionally graded plates and shells. *Composites Part B: Engineering,* vol. 42, pp. 123-133.

Carrera, E.; Brischetto, S.; Robaldo, A. (2008): Variable kinematic model for the analysis of functionally graded material plates. *AIAA journal,* vol. 46, pp. 194-203.

Chen, C.-S.; Hsu, C.-Y.; Tzou, G. J. (2009): Vibration and stability of functionally graded plates based on a higher-order deformation theory. *Journal of Reinforced Plastics and Composites,* vol. 28, pp. 1215-1234.

Chen, W.-H.; Wu, C.-W. (1995): A spline wavelets element method for frame structures vibration. *Computational Mechanics,* vol. 16, pp. 11-21.

Chen, W. H.; Wu, C. W. (1996): Adaptable spline element for membrane vibration analysis. *International journal for numerical methods in engineering,* vol. 39, pp. 2457-2476.

Cheng, Z.-Q.; Batra, R. (2000): Exact correspondence between eigenvalues of membranes and functionally graded simply supported polygonal plates. *Journal of Sound and Vibration,* vol. 229, pp. 879-895.

Cheung, Y.;Zhang, Y.; Wanji, C. (2000): The application of a refined nonconforming quadrilateral plate bending element in thin plate vibration and stability analysis. *Finite elements in Analysis and Design,* vol. 34, pp. 175-191.

Civalek, O.; Acar, M. H. (2007): Discrete singular convolution method for the analysis of Mindlin plates on elastic foundations. *International Journal of Pressure Vessels and Piping,* vol. 84, pp. 527-535.

Dong, L.; Atluri, S. (2011): A simple procedure to develop efficient & stable hybrid/mixed elements, and Voronoi cell finite elements for macro-& micromechanics. *Computers Materials and Continua,* vol. 24, pp. 61.

Dong, L.; El-Gizawy, A. S.; Juhany, K. A.; Atluri, S. N. (2014a): A Sim-

ple Locking-Alleviated 3D 8-Node Mixed-Collocation C 0 Finite Element with Over-Integration, for Functionally-Graded and Laminated Thick-Section Plates and Shells, with & without Z-Pins. *CMC: Computers Materials and Continua*, vol. 41, pp. 163-192.

Dong, L.; El-Gizawy, A. S.; Juhany, K. A.; Atluri, S. N. (2014b): A Simple Locking-Alleviated 4-Node Mixed-Collocation Finite Element with Over-Integration, for Homogeneous or Functionally-Graded or Thick-Section Laminated Composite Beams. *CMC: Computers, Materials & Continua,* vol. 40, pp. 49-77.

Ersoy, H.; Civalek, Ö; Guerses, M. (2009): Discrete singular convolution method for buckling analysis of rectangular Mindlin plates. *The IES Journal Part A: Civil & Structural Engineering,* vol. 2, pp. 143-152.

Ferreira, A.; Batra, R.; Roque, C.; Qian, L.; Martins, P. (2005): Static analysis of functionally graded plates using third-order shear deformation theory and a meshless method. *Composite Structures,* vol. 69, pp. 449-457.

Ferreira, A. J.; Roque, C.; Jorge, R.; Fasshauer, G.; Batra, R. (2007): Analysis of functionally graded plates by a robust meshless method. *Mechanics of Advanced Materials and Structures,* vol. 14, pp. 577-587.

Gilhooley, D.; Batra, R.; Xiao, J.; Mccarthy, M.; Gillespie Jr, J. (2007): Analysis of thick functionally graded plates by using higher-order shear and normal deformable plate theory and MLPG method with radial basis functions. *Composite Structures,* vol. 80, pp. 539-552.

Hall, W. S. (1994): *Boundary Element Method*, Springer.

Hartmann, R.; Houston, P. (2002): Adaptive discontinuous Galerkin finite element methods for the compressible Euler equations. *Journal of Computational Physics,* vol. 183, pp. 508-532.

Hinton, E. (1988): *Numerical methods and software for dynamic analysis of plates and shells*, Pineridge Press.

Hosseini-Hashemi, S.; Fadaee, M.; Atashipour, S. (2011a): A new exact analytical approach for free vibration of Reissner–Mindlin functionally graded rectangular plates. *International Journal of Mechanical Sciences,* vol. 53, pp. 11-22.

Hosseini-Hashemi, S.; Fadaee, M.; Atashipour, S. (2011b): Study on the free vibration of thick functionally graded rectangular plates according to a new exact closed-form procedure. *Composite Structures,* vol. 93, pp. 722-735.

Hosseini-Hashemi, S.; Rokni Damavandi Taher, H.; Akhavan, H.; Omidi, M. (2010): Free vibration of functionally graded rectangular plates using first-order shear deformation plate theory. *Applied Mathematical Modelling,* vol. 34, pp. 1276-1291.

Huang, X.-L.; Shen, H.-S. (2004): Nonlinear vibration and dynamic response of functionally graded plates in thermal environments. *International Journal of Solids and Structures,* vol. 41, pp. 2403-2427.

Jiawei, X.; Xuefeng, C.; Zhengjia, H.; Yinghong, Z. (2008): A new wavelet-based thin plate element using B-spline wavelet on the interval. *Computational Mechanics,* vol. 41, pp. 243-255.

Koizumi, M. (1997): FGM activities in Japan. *Composites Part B: Engineering,* vol. 28, pp. 1-4.

Liew, K.; Chen, X. (2004): Mesh-free radial point interpolation method for the buckling analysis of Mindlin plates subjected to in-plane point loads. *International Journal for Numerical Methods in Engineering,* vol. 60, pp. 1861-1877.

Liew, K.; Yang, J.; Kitipornchai, S. (2003): Postbuckling of piezoelectric FGM plates subject to thermo-electro-mechanical loading. *International Journal of Solids and Structures,* vol. 40, pp. 3869-3892.

Matsunaga, H. (2008): Free vibration and stability of functionally graded plates according to a 2-D higher-order deformation theory. *Composite structures,* vol. 82, pp. 499-512.

Merdaci, S.; Tounsi, A.; Houari, M. S. A.; Mechab, I.; Hebali, H.; Benyoucef, S. (2011): Two new refined shear displacement models for functionally graded sandwich plates. *Archive of Applied Mechanics,* vol. 81, pp. 1507-1522.

Mindlin, R. D. (1951): Influence of rotary inertia and shear on flexural motions of isotropic, elastic plates. *J. of Appl. Mech.,* vol. 18, pp. 31-38.

Mindlin, R. D.; Schacknow, A.; Deresiewicz, H. (1955). Flexural vibrations of rectangular plates. DTIC Document.

Mohammadi, M.; Saidi, A. R.; Jomehzadeh, E. (2010): Levy solution for buckling analysis of functionally graded rectangular plates. *Applied Composite Materials,* vol. 17, pp. 81-93.

Natarajan, S.; Manickam, G. (2012): Bending and vibration of functionally graded material sandwich plates using an accurate theory. *Finite Elements in Analysis and Design,* vol. 57, pp. 32-42.

Neves, A.; Ferreira, A.; Carrera, E.; Cinefra, M.; Roque, C.; Jorge, R.; Soares, C. (2013): Static, free vibration and buckling analysis of isotropic and sandwich functionally graded plates using a quasi-3D higher-order shear deformation theory and a meshless technique. *Composites Part B: Engineering,* vol. 44, pp. 657-674.

Neves, A.; Ferreira, A.; Carrera, E.; Roque, C.; Cinefra, M.; Jorge, R.; Soares, C. (2012): A quasi-3D sinusoidal shear deformation theory for the static and free vibration analysis of functionally graded plates. *Composites Part B: Engineering,*

vol. 43, pp. 711-725.

Nguyen-Xuan, H.; Rabczuk, T.; Nguyen-Thanh, N.; Nguyen-Thoi, T.; Bordas, S. (2010): A node-based smoothed finite element method with stabilized discrete shear gap technique for analysis of Reissner–Mindlin plates. *Computational mechanics,* vol. 46, pp. 679-701.

Purbolaksono, J.; Aliabadi, M. (2005): Buckling analysis of shear deformable plates by boundary element method. *International journal for numerical methods in engineering,* vol. 62, pp. 537-563.

Qian, L.; Batra, R.; Chen, L. (2004): Static and dynamic deformations of thick functionally graded elastic plates by using higher-order shear and normal deformable plate theory and meshless local Petrov–Galerkin method. *Composites Part B: Engineering,* vol. 35, pp. 685-697.

Shariat, B.; Eslami, M. (2007): Buckling of thick functionally graded plates under mechanical and thermal loads. *Composite Structures,* vol. 78, pp. 433-439.

Shariat, B.; Javaheri, R.; Eslami, M. (2005): Buckling of imperfect functionally graded plates under in-plane compressive loading. *Thin-walled structures,* vol. 43, pp. 1020-1036.

Singha, M.; Prakash, T.; Ganapathi, M. (2011): Finite element analysis of functionally graded plates under transverse load. *Finite elements in Analysis and Design,* vol. 47, pp. 453-460.

Talha, M.; Singh, B. (2010): Static response and free vibration analysis of FGM plates using higher order shear deformation theory. *Applied Mathematical Modelling,* vol. 34, pp. 3991-4011.

Thai, H.-T.; Choi, D.-H. (2013): A simple first-order shear deformation theory for the bending and free vibration analysis of functionally graded plates. *Composite Structures,* vol. 101, pp. 332-340.

Thai, H.-T.; Park, T.; Choi, D.-H. (2013): An efficient shear deformation theory for vibration of functionally graded plates. *Archive of Applied Mechanics,* vol. 83, pp. 137-149.

Thai, H.-T.; Vo, T. P. (2013): A new sinusoidal shear deformation theory for bending, buckling, and vibration of functionally graded plates. *Applied mathematical modelling,* vol. 37, pp. 3269-3281.

Timoshenko, S. P.; Gere, J. M. (2012): *Theory of elastic stability*, Courier Dover Publications.

Tounsi, A.; Houari, M. S. A.; Benyoucef, S.; Adda Bedia, E. A. (2013): A refined trigonometric shear deformation theory for thermoelastic bending of functionally graded sandwich plates. *Aerospace Science and Technology,* vol. 24, pp.

209-220.

Uymaz, B.; Aydogdu, M. (2007): Three-dimensional vibration analyses of functionally graded plates under various boundary conditions. *Journal of Reinforced Plastics and Composites,* vol. 26, pp. 1847-1863.

Wu, C.-P.; Li, H.-Y. (2010): An RMVT-based third-order shear deformation theory of multilayered functionally graded material plates. *Composite Structures,* vol. 92, pp. 2591-2605.

Xiang, J.; Chen, X.; He, Y.; He, Z. (2006): The construction of plane elastomechanics and Mindlin plate elements of B-spline wavelet on the interval. *Finite elements in analysis and design,* vol. 42, pp. 1269-1280.

Xiang, J.; Chen, X.; He, Z.; Dong, H. (2007): The construction of 1D wavelet finite elements for structural analysis. *Computational Mechanics,* vol. 40, pp. 325-339.

Yang, J.; Liew, K.; Kitipornchai, S. (2005): Second-order statistics of the elastic buckling of functionally graded rectangular plates. *Composites science and technology,* vol. 65, pp. 1165-1175.

Yang, J.; Shen, H.-S. (2001): Dynamic response of initially stressed functionally graded rectangular thin plates. *Composite Structures,* vol. 54, pp. 497-508.

Yang, Z.; Chen, X.; Zhang, X.; He, Z. (2013): Free vibration and buckling analysis of plates using B-spline wavelet on the interval Mindlin element. *Applied Mathematical Modelling,* vol. 37, pp. 3449-3466.

Zenkour, A. (2005a): A comprehensive analysis of functionally graded sandwich plates: Part 1—Deflection and stresses. *International Journal of Solids and Structures,* vol. 42, pp. 5224-5242.

Zenkour, A. (2005b): A comprehensive analysis of functionally graded sandwich plates: Part 2—Buckling and free vibration. *International Journal of Solids and Structures,* vol. 42, pp. 5243-5258.

Zenkour, A. M. (2006): Generalized shear deformation theory for bending analysis of functionally graded plates. *Applied Mathematical Modelling,* vol. 30, pp. 67-84.

Zhao, X.; Lee, Y.; Liew, K. (2009a): Free vibration analysis of functionally graded plates using the element-free< i> kp</i>-Ritz method. *Journal of Sound and Vibration,* vol. 319, pp. 918-939.

Zhao, X.; Lee, Y.; Liew, K. (2009b): Mechanical and thermal buckling analysis of functionally graded plates. *Composite Structures,* vol. 90, pp. 161-171.

Zhong, Y.; Xiang, J. (2011): Construction of wavelet-based elements for static and stability analysis of elastic problems. *Acta Mechanica Solida Sinica,* vol. 24, pp. 355-364.

Zhu, P.; Liew, K. (2011): Free vibration analysis of moderately thick functionally graded plates by local Kriging meshless method. *Composite Structures,* vol. 93, pp. 2925-2944.

Zuo, H.; Yang, Z.; Chen, X. (in press): Static, free vibration and buckling analysis of functionally graded beam via B-spline wavelet on the interval and Timoshenko beam theory. *CMES: Computer Modeling in Engineering and Sciences*.

Appendix

$$\mathbf{\Gamma}_x^{0,0} = l_{ex} \int_0^1 \mathbf{T}^T \mathbf{\Phi}^T \mathbf{\Phi} \mathbf{T} \mathrm{d}\xi \tag{A1}$$

$$\mathbf{\Gamma}_x^{0,1} = \int_0^1 \mathbf{T}^T \mathbf{\Phi}^T \frac{\mathrm{d}\mathbf{\Phi}}{\mathrm{d}\xi} \mathbf{T} \mathrm{d}\xi \tag{A2}$$

$$\mathbf{\Gamma}_x^{1,0} = \int_0^1 \mathbf{T}^T \frac{\mathrm{d}\mathbf{\Phi}^T}{\mathrm{d}\xi} \mathbf{\Phi} \mathbf{T} \mathrm{d}\xi \tag{A3}$$

$$\mathbf{\Gamma}_x^{1,1} = \frac{1}{l_{ex}} \int_0^1 \mathbf{T}^T \frac{\mathrm{d}\mathbf{\Phi}^T}{\mathrm{d}\xi} \frac{\mathrm{d}\mathbf{\Phi}}{\mathrm{d}\xi} \mathbf{T} \mathrm{d}\xi \tag{A4}$$

$$\mathbf{\Gamma}_y^{0,0} = l_{ey} \int_0^1 \mathbf{T}^T \mathbf{\Phi}^T \mathbf{\Phi} \mathbf{T} \mathrm{d}\eta \tag{A5}$$

$$\mathbf{\Gamma}_y^{0,1} = \int_0^1 \mathbf{T}^T \mathbf{\Phi}^T \frac{\mathrm{d}\mathbf{\Phi}}{\mathrm{d}\eta} \mathbf{T} \mathrm{d}\eta \tag{A6}$$

$$\mathbf{\Gamma}_y^{1,0} = \int_0^1 \mathbf{T}^T \frac{\mathrm{d}\mathbf{\Phi}^T}{\mathrm{d}\eta} \mathbf{\Phi} \mathbf{T} \mathrm{d}\eta \tag{A7}$$

$$\mathbf{\Gamma}_y^{1,1} = \frac{1}{l_{ex}} \int_0^1 \mathbf{T}^T \frac{\mathrm{d}\mathbf{\Phi}^T}{\mathrm{d}\eta} \frac{\mathrm{d}\mathbf{\Phi}}{\mathrm{d}\eta} \mathbf{T} \mathrm{d}\eta \tag{A8}$$